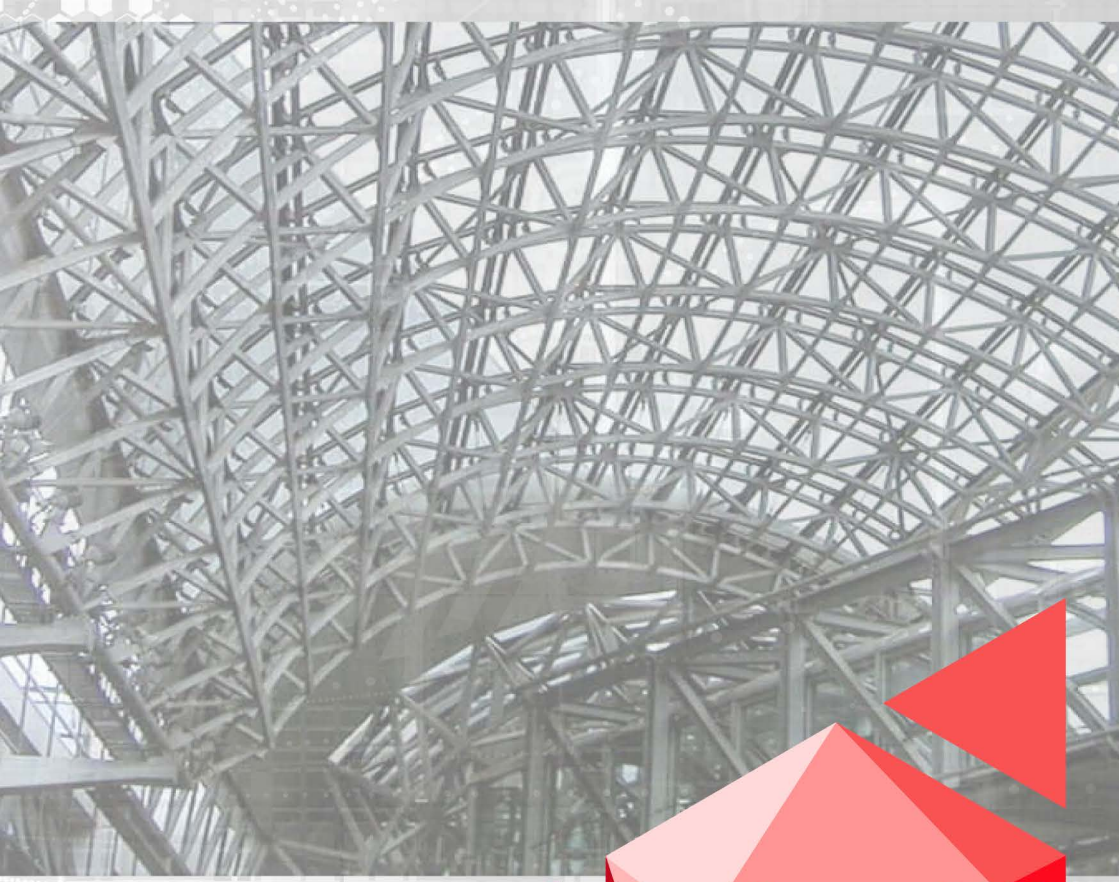

Warsaw 2022

ENERGY-SAVING TECHNOLOGIES MANUFACTURING OF METAL STRUCTURES WITH CORE ELEMENTS

S. M. OSPANOVA

ENERGY-SAVING TECHNOLOGIES MANUFACTURING OF METAL STRUCTURES WITH CORE ELEMENTS

MONOGRAPH

S. M. OSPANOVA

RS Global
Warsaw, Poland
2022

DOI: 10.31435/rsglobal/047

S.M. Ospanova

Energy-saving technologies manufacturing of metal structures with core elements. Monograph. – Warsaw: RS Global Sp. z O.O., 2022. – 84 c.

ISBN 978-83-962343-9-1 (eBook)

The monograph analyzes various welded metal structures. The design of reinforcing cages of round, hot-rolled, cold-rolled, cold-flattened steel of periodic profile has been studied. During the welding process, the possibility of splashes has been established that affects the strength of the welded joint, and is associated with large energy losses. This phenomenon is accepted as an indicator of the quality of the welding process.

The process of heating by contact welding of crossed round rods is described. It was found that the higher the current, the relatively later the limiting state sets in, the shorter the welding duration and the less the possibility of overheating the near-contact region.

Issues of rational technology of resistance welding of reinforced concrete reinforcement have been developed. The parameters of the mode of electric contact welding of crossing round rods are determined.

The publication may be of interest to a wide range of readers interested in the problem of studying energy-saving technologies for the manufacture of metal structures with rod elements, including researchers, teachers and students of higher educational institutions in the field of energy conservation.

ISBN 978-83-962343-9-1 (eBook)

TABLE OF CONTENTS

INTRODUCTION

In industrial and civil construction, as well as in the construction of roads and tunnels, reinforced concrete structures are widely used, especially non-stressed reinforced concrete structures. These structures are mainly manufactured in the factory.

In reinforced concrete structures, rods made of low-carbon steel of various profiles are used in the form of round rods (reinforcement). In non-stressed structures, round rods of small diameter up to 10 mm are used. For reinforced concrete structures, metal meshes are made from them by electrocontact welding. Metal meshes are made from rods of both the same diameter and from rods of different diameters.

70% of the generated electricity is spent on the manufacture of products of various electrical technologies, including the manufacture of metal nets for reinforced concrete structures by the electrocontact method.

When electrocontact welding of a metal structure for reinforced concrete, quality control methods are not applied. Only the compliance of the technical properties of the welded rods is checked by the method of their tensile testing. When developing the technology of electrocontact welding of rods in the creeks, they try to achieve equal-strength joints of the corresponding base metal, which is achieved by significantly increasing the welding current by significant overheating of the molten metal in the welding zone.

At the same time, when assessing the quality, our studies show that the samples welded according to the factory technology failed not along the welded point, but along the base metal. Based on this, after reaching the melting point of the base metal in the welding zone, an increase in the welding current according to the factory technology is impractical.

The development of an energy-saving technology for electric contact welding of crossed rods, which implies the determination of the parameters of the welding mode, including the welding current, which ensures the achievement of the melting temperature of the material to be welded in the welding zone.

When electrocontact welding of metal structures, the strength of the weld depends on the value of the welding current. At the same time, the value of the welding current and the strength of the welded joint significantly depend on the compressive force between the electrodes and the duration of welding. The purpose of this work is to develop an energy-saving technology for electric contact welding of metal structures, which implies the determination of the smallest value of the welding current required to ensure maximum strength during welding, as well as other parameters of the welding mode.

CHAPTER 1. WELDED METAL CONSTRUCTIONS APPLIED IN REINFORCED CONCRETE CONSTRUCTIONS IN CONSTRUCTION

Reinforced concrete structures are the backbone of the modern construction industry. They are used: in industrial, civil and agricultural construction − for buildings for various purposes; in transport construction − for subways, bridges, tunnels; in energy construction − for hydroelectric power plants, nuclear reactors, etc.

This widespread use in construction reinforced concrete has received due to its many positive properties: durability, fire resistance, resistance to weathering, high resistance to static and dynamic loads, low operating costs for the maintenance of buildings and structures, etc. Reinforced concrete is a building material in which they are connected to monolithic whole hardened concrete and steel reinforcement. In reinforced concrete, compressive loads are perceived by concrete, and tensile forces - by steel reinforcement [1-6].

Depending on the construction methods and purpose, reinforced concrete is of three types: monolithic, precast and precast-monolithic. The paper considers two types of reinforced concrete: precast and monolithic, evaluates the positive and negative qualities of these materials and presents their comparative analysis.

The main advantages of reinforced concrete, ensuring its widespread use in construction, include [7-11]:

- fire resistance;
- durability;
- high mechanical strength in compression;
- good resistance to seismic and other dynamic influences;
- the ability to build structures of any shape;
- low operating costs for the maintenance of buildings and structures (in comparison with metal and wooden structures);
- good resistance to weathering;
- high hygiene, the ability to trap radioactive radiation;
- almost ubiquitous presence of large and small aggregates, in large quantities used for the preparation of concrete.

All these factors make reinforced concrete available for use almost throughout the country. The cost of electricity for the production of reinforced concrete structures is much lower in comparison with steel and stone ones.

Disadvantages of reinforced concrete [12-15]:

- high density (large dead weight);
- high sound and thermal conductivity;
- labor intensity of alterations and reinforcements;
- the need for holding the structure in the formwork before the concrete acquires the required strength;
- the appearance of cracks due to shrinkage and force effects.
- the need for holding the structure in the formwork before the concrete acquires the required strength;
- the appearance of cracks due to shrinkage and force effects.

Many of these drawbacks can be fully or partially eliminated by using concretes with porous fillers, special processing (steaming, evacuation, etc.), pre-stressing.

With a general assessment of reinforced concrete as a building material, it should be borne in mind that the disadvantages noted above are insignificant in comparison with its advantages. This led to the fact that in a historically short period of time (about 150 years), reinforced concrete took a dominant position in construction.

For modern capital construction, reinforced concrete is the building material № 1. Depending on the methods of construction, reinforced concrete structures are distinguished [16-20]:

- prefabricated, predominantly manufactured at factories of the building industry and then assembled at construction sites;
- monolithic, fully erected at the construction site;
- precast-monolithic, in which the use of prefabricated prefabricated reinforced concrete elements and monolithic parts of structures is rationally combined.

Reinforced concrete structures are distinguished by the type of reinforcement:

- with flexible fittings (without prestressing and with prestressing);
- with rigid (bearing) reinforcement.

Reinforced concrete is used in a wide variety of construction industries, finding in each of them its own suitable areas of application. Reinforced concrete is used:

- during the construction of residential buildings, public buildings for various purposes, agricultural buildings;
- during the construction of buildings and structures for industrial, civil and transport purposes [21];
- in hydrotechnical construction (dams, dams, hydroelectric power plants) and energy construction (for the construction of the main buildings of thermal and nuclear power plants, nuclear reactors);
- during the construction of various engineering structures (chimneys, television and water towers, reservoirs, etc.);
- in transport construction (for the construction of bridges, culverts, overpasses, subways, tunnels on railways and highways, retaining walls, for covering roads and airfields, reinforced concrete sleepers, reinforced concrete supports of the contact network);
- in the mining industry for mine structures and fastening of underground workings;
- often in shipbuilding (for example, barge hulls are made of reinforced concrete) and mechanical engineering (for the manufacture of beds and supporting parts of heavy machines and presses).

In recent decades, reinforced concrete began to be used in the cocking of platforms for oil extraction from the seabed in the shelf zone and for the construction of sarcophagi and space suits for the disposal of radioactive waste and storage of radioactive materials.

Forecasts show that in the current century, reinforced concrete will remain the main building material for load-bearing and enclosing structures of buildings and structures for various purposes.

Reinforced concrete products are the most durable and strong structures in construction. Due to the use of metal reinforcement in the manufacture of reinforced concrete products (reinforced concrete products), their resistance significantly exceeds alternative materials and retains resistance to corrosion. Depending on the application of concrete products, their designs may vary. The basis for concrete goods can be both Portland cement and silicate concrete. Figure 1.1 shows some types of concrete products.

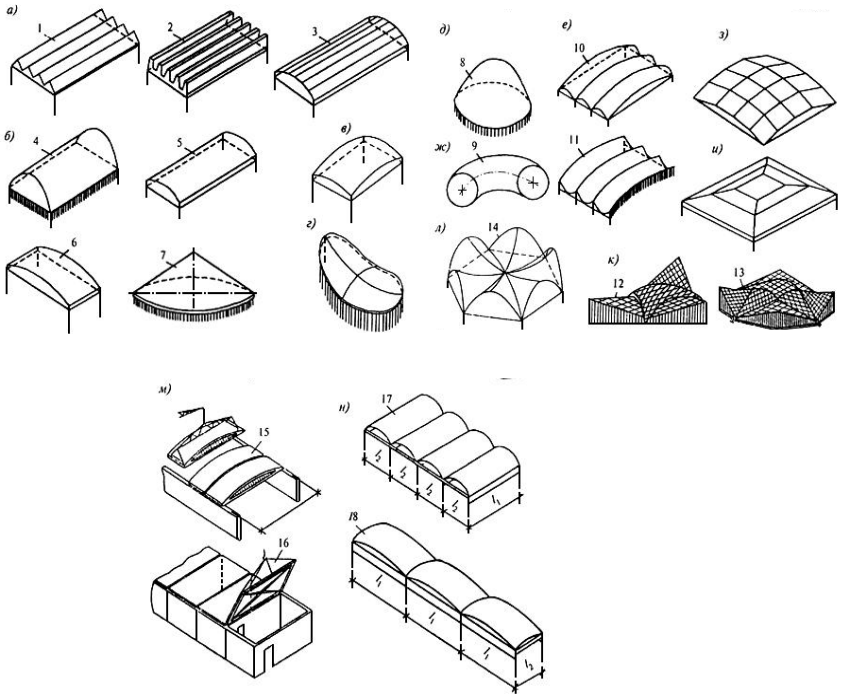

Figure 1.1. Types of reinforced concrete structures

a − prismatic folds; b − shells of zero Gaussian curvature; c − shells of positive Gaussian curvature; d − the same, negative; d − shells with a vertical axis of rotation; e − shells with a horizontal axis of rotation; g − toroidal shells of ambiguous Gaussian curvature; z − polyhedra; i − the same, tent-type; k − composite shells; l − the same, from hyperbolic triangular arches; m − shell panels; KZHS the size of the span of the coating and the broken shells the size of the cell of the building; h − continuous shells; 1 − beam fold with triangular cross-section; 2 − the same, with trapezoidal; 3 − the same, with vaulted (prismatic convex folds); 4 − arch-shell; 5 − long cylindrical shells, 6 − the same, short; 7 − conical shell; 8 − dome; 9 − toroidal shell; 10 − barrel vaults; 11 − hyperbolic shells; 12 − covering with a triangular plan of shells of positive and negative Gaussian curvature; 13 − the same, with a polygonal plan; 14 − coating of composite hypars; 15 − panels-shells of KZHS; 16 – broken plates-shells; 17 – multi-wave shells; 18 − multi-span shells.

Currently, the precast concrete industry is quite developed, and such factories can be found in many countries, and with the development of Internet technology, more and more opportunities appear to purchase precast concrete products remotely. For example, such an opportunity in Ukraine is provided by the Kiev Reinforced Concrete Plant DBK4. Today, construction cannot be imagined without the use of concrete products, therefore the company offers its customers a variety of plates, blocks, panels, lintels and much more.

Among the advantages of using reinforced concrete products are excellent thermal insulation properties and efficiency. Using finished products, you don't have to import it, hire concrete mixing machines, and besides, you don't have to wait until it hardens. Thus, not only time is saved, but also money. The use of reinforced concrete products is not limited by the weather, therefore, the use of reinforced concrete products remains possible at any time of the year.

In addition, it is very convenient to build a house from reinforced concrete wall blocks, unlike other materials. The unique production technology ensures excellent quality and reliability of the structure, and the process of assembling the blocks is quick and cheap.

Precast reinforced concrete in construction practice is widespread, it is used on a par with steel, with the exception of those areas where its use is impractical or impossible. The raw materials for reinforced concrete are concrete and reinforcement. The current building codes for concrete and reinforced concrete structures allow the use of nineteen classes of concrete, seven classes of bar reinforcement and five classes of wire.

Prefabricated reinforced concrete structures are manufactured at the factories of reinforced concrete products, and the finished structures are assembled at the construction site, i.e. set in the design position. Precast concrete is widely used in industrial, civil, rural, hydraulic engineering, mine, transport, energy and other types of construction.

The disadvantage of the factory manufacturing method is the inability to produce a wide range of designs. This is especially true for the variety of forms of manufactured structures, which are limited to typical formwork. In fact, at precast concrete factories, only structures that require mass use are made. In light of this circumstance, the widespread introduction of precast concrete technology leads to the emergence of a large number of similar buildings.

The use of prefabricated reinforced concrete structures in construction allows you to increase the productivity of workers, improve the quality and durability of buildings and structures, reduce the time of their construction and reduce the consumption of steel [15, 17, 21].

Monolithic reinforced concrete structures are erected with the execution of formwork, installation of reinforcing cages and laying of concrete mixture at the construction site. After the concrete has acquired sufficient strength (usually after 7 days), the formwork is disassembled. For a monolithic foundation, high-strength concrete and reinforcement with a diameter of at least 12 mm are used. Such a

foundation is used on highly compressible soils (peat bogs, sand cushions, etc.) and is rightfully considered the most versatile and reliable. The monolithic foundation differs from other varieties by the presence of a massive concrete slab, which makes up a single structure with formwork.

To protect such reinforced concrete structures, special polymer compositions are used to isolate the surface layer of reinforced concrete from the negative influences of the external environment. To protect the reinforced concrete base, various types of protective structures are used, which make it possible to modify the operational properties of the mineral surface − to increase wear resistance, reduce dust separation, impart decorative properties (color and degree of gloss), and improve chemical resistance.

Another method of protecting reinforced concrete structures is to coat the reinforcement with zinc phosphate, which slowly reacts with a corrosive chemical (such as alkali) to form a stable coating.

To protect reinforced concrete structures from the effects of water and aggressive environments, penetrating waterproofing is also used, which modifies the structure of concrete, increasing its water resistance, which prevents the destruction of concrete structures and corrosion of reinforcement.

Rational areas of application of monolithic reinforced concrete are hydraulic structures, road and airfield pavements, foundations for industrial equipment, tanks, towers, elevators, etc. Solid foundations and special structures (dams, chimneys) are usually erected from monolithic reinforced concrete, and in recent years, residential buildings, hotels and other buildings.

The use of precast concrete reduces the cost of construction by reducing the consumption of concrete, steel and timber and provides an increase in labor productivity. Precast concrete can significantly increase the structural efficiency of a building − the length of spans, the area of open spaces, reduce the thickness of structures and diversify the layout of living quarters.

The advantages of monolithic reinforced concrete structures include their durability and fire resistance, the ability to form products of the required shape, high rigidity, the ability to use local materials, and steel savings. The use of monolithic reinforced concrete structures allows you to significantly expand the possibilities in the process of internal planning of residential premises. Monolithic reinforced concrete has high thermal insulation characteristics. The construction of monolithic buildings has another very important advantage − in the first years after construction, the object subsides completely, without forming cracks [18, 19, 21].

It should be noted, for example, the disadvantages of foundations made of precast concrete elements, which consist in the fact that in low-rise construction, blocks intended for 9-12-storey buildings are used irrationally with a decrease in the number of floors. Their bearing capacity is used no more than 10%. A lot of people and expensive equipment are involved in the manufacture of foundation blocks, their transportation and installation.

Therefore, the achievement of a reduction in construction time is due to the deterioration of other indicators. Individual blocks of a prefabricated foundation

cannot withstand the applied loads with sufficient efficiency, and with large settlements of the foundation, irreversible deformations and destruction appear in the building frame.

Disadvantages of monolithic reinforced concrete structures: large dead weight, the need for scaffolding and formwork, high labor intensity of construction, maintaining the manufactured structure in the formwork until the concrete acquires the required strength.

It is impossible to unequivocally answer the question of which type of reinforced concrete is better − precast or monolithic. Obviously, one material has its own advantages, while the other has its own. But several points can be noted, on which the differences between these materials are clearly visible:

– prefabricated reinforced concrete has significant advantages over monolithic, as it allows the widespread introduction of industrialization in the construction business (progressive technological methods of manufacturing products in factories and mechanized installation of structures);

– material costs in the construction of prefabricated foundations are 50-75% higher than the material costs of monolithic structures;

– a foundation made of precast concrete blocks loses in strength and other operational characteristics to a monolithic foundation [14, 17, 18];

– construction using precast concrete products is in some cases inapplicable, for example, in cramped conditions during construction in the city center, where it is not possible, for example, to provide a site for storing materials;

– construction using precast concrete products is in some cases inapplicable, for example, in cramped conditions during construction in the city center, where it is not possible, for example, to provide a site for storing materials;

– during construction from monolithic reinforced concrete, the consumption of reinforcement is reduced by 2-5 times in comparison with construction from precast concrete.

The armature, used in reinforced concrete structures and structures, is divided into working, distribution, clamps and assembly (Figure 1.2).

Working reinforcement absorbs tensile and shear forces arising in reinforced concrete from external loads and the own weight of structures.

Distribution reinforcement holds the working reinforcement rods in a certain position and distributes the load between them.

In those cases when the working rods are located not only in tensioned, but also in compressed parts of structures, for example, in beams, girders, the reinforcement is called double. The clamps tie the reinforcement into a single frame and protect the concrete from the appearance of oblique cracks near the supports. Mounting reinforcement does not perceive any efforts, serves to assemble the reinforcement cage and ensures the exact position of the working reinforcement and clamps during concreting.

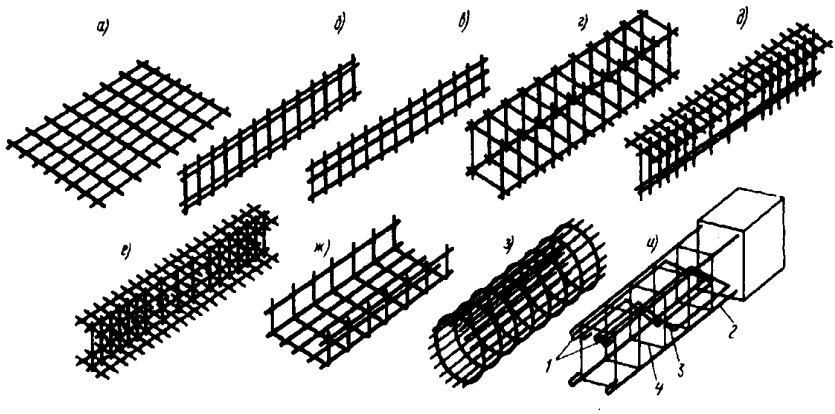

Figure 1.2. Basic structures of reinforced concrete metal reinforcement a- mesh, b- longitudinal frame, c- frame with additional reinforcement, g-, d-, T-frame, e-I-frame, y- clamps, h- round frame, and- frame with clamps.

For better protection of the reinforcement against sliding in concrete, the tensile rebars are bent in the form of hooks at the ends. Due to the increased adhesion to concrete, the use of rebars with a periodic profile makes it possible in most cases to abandon hooks, which leads to savings in steel.

According to the method of installation, fittings are subdivided into types: piece fittings, reinforcing meshes, reinforcing cages, reinforcing structures [15, 21].

Piece fittings can be bar (from round rods) and rigid (from profile rolled steel: I-beams, channels, angles, rails, pipes). Piece reinforcement is assembled by welding at the place of concreting into a reinforcing cage or reinforcing structure from individual elements. The use of piece reinforcement is advisable for small volumes of work, if it is necessary to fit the rods in place in the cramped conditions of the concreted structure.

Reinforcing mesh is a mutually intersecting rods connected at the intersection by welding or tack, and is mainly used for reinforcing slabs. Reinforcement cages usually consist of longitudinal reinforcement and a grid connecting them. These are the so-called flat frames. Another type of reinforcing cages are lattice cages, assembled from several flat cages or flat meshes and bags. Reinforcement cages are used to reinforce beams, columns, etc.

For the manufacture of reinforcing cages, round, hot-rolled, cold-rolled, cold-flattened steel of a periodic profile is used.

Reinforcing bars are produced by rolling at metallurgical plants. Wire reinforcement is obtained by cold drawing of rolled rods through a system of successively decreasing holes - dies. As a result of repeated pulling, the diameter of the rod decreases and its length increases.

This changes the crystal structure of the steel and significantly increases its tensile strength. Depending on the method of subsequent hardening, the rod reinforcement can be thermally hardened (heat treated) or draw hardened (cold drawn).

It should be noted that, in addition to metal fittings, non-metallic ones are also used.

According to the profile, the reinforcement is divided into round, smooth and periodic profile reinforcement. Reinforcement bars are uniformly grooved rods to improve adhesion to concrete. Reinforcement with a periodic profile with two longitudinal ribs and transverse protrusions running along a three-start helical line is produced. The smooth reinforcement has no corrugation.

According to the principle of operation, the fittings are divided into non-stressed and pre-stressed ones.

Welding of meshes and fabrication of mesh products from wire by resistance welding is a widespread field of application of resistance welding [22-25]. Welding of meshes and mesh products is possible both on standard resistance welding machines and on fully equipped mesh welding lines. With the outward simplicity of the technology of the process and the device of equipment for welding meshes, there are many specifics due to both the serial production or mass production, and the wire used.

If, when welding meshes for reinforcing reinforced concrete slabs, GOST relatively clearly describes the requirements for the quality of welding, then in the manufacture of mesh products, such as fences, cable trays, various baskets and frames, racks, there is no clear standardization of the quality indicators of mesh production. Let us consider some of the features of resistance welding in relation to the production of products from welded mesh.

From the point of view of the consumer, the welded mesh should have normal geometry, right angles, the required arrangement of longitudinal and transverse rods, be flat and have the strength of welded joints sufficient for bending the mesh without destroying them, and, in addition, the welded mesh should not have noticeable traces of deformation, splashes and sharp burr - this causes difficulties for high-quality painting or coating of a welded mesh product or mesh, and can also cause injury to the consumer of the finished product. There are some technological features when welding such meshes.

It is not always possible to use cheap wire for the manufacture of mesh, which has disadvantages. There is a reasonable limit here. If you weld wires crosswise in hard welding modes, this usually gives the best appearance, good strength properties in combination with high productivity.

But with a dirty surface or a deviation of the wire diameter, welding with stable quality in hard modes becomes impossible - you have to move to the area of a softer welding mode. Until a certain moment, this does not affect the appearance of the welded mesh, but it already entails a certain decrease in strength properties. With a further decrease in the current and forced drift towards even whiter softer

modes, heating and general deformation of the bars in the welding zone occurs - the mesh loses flatness

Considering the large number of welds of mesh crosshairs, even with an increase in the total welding cycle time by 3-4 network periods, welding a square meter of mesh with a mesh of 40x40 mm will last 35-50 seconds longer. When using even manual welding of a mesh on a stationary machine in a rigid mode, the production of such a mesh map takes about 6 minutes. When using wires with mediocre surface quality, mesh welding performance drops by at least 10%. The above is related to the use of wire mesh made of low carbon steels for welding and is not always true in the case of using alloy and stainless steels [26-29].

At factories of manufacturers of reinforced concrete metal structures, the quality is checked by assessing the mechanical properties of reinforcement by tensile testing, and there is still no quality assessment criterion. For the development of energy-saving technology, it becomes necessary that we develop criteria for assessing the quality of electrical contact welded joints of crossed rods.

In resistance welding, the dimensions of the cast core are often used as such a criterion. However, when welding a metal mesh from reinforcing bars, depending on the welding mode, joints can form with the core in the liquid phase, as well as in the solid phase without the formation of a cast core. In these cases, it is advisable to use the results of mechanical tests of the welded joint as a criterion for the quality of reinforcement welding.

In non-stressed reinforced concrete structures, both tearing and shearing forces act on the welded joint due to the physical and mechanical effects of concrete. In this regard, the quality criterion for resistance welding of reinforcement can be the results of mechanical tests of welded joints for pull-off and shear (Figure 1.3).

To compare the test schemes (Figure 1.3), 20 samples were welded at different values of the welding current. Welding was carried out under optimal and constant mode parameters and conditions. Ten samples from each batch were tested for strength according to two investigated schemes (Table 1.1).

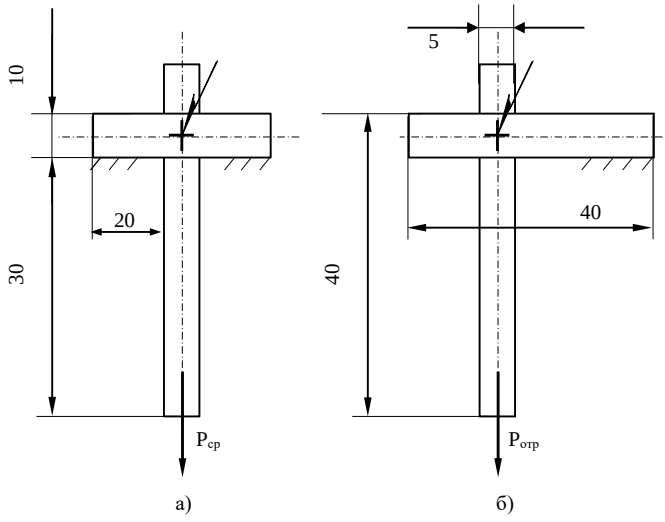

Figure 1.3. Schemes for testing welded joints for shear (a) and pull-off (b).

Table 1.1. Experimental and calculated data for calculating the correlation coefficient between the welding current (I1, I2) and the mechanical pull-off and shear test of the welded joint

№	On a slice						On the breakaway			
	Pср,Y1, даН	Pсв, Y1, кА	Y_1^2	X_1^2	Y1 X1	Pотр, Y2, даН	I2, X2, кА	Y_2^2	X_2^2	Y2 X2
1	16,6	1,0	275,56	1,0	16,6	13,1	1,1	171,61	1,21	14,41
2	17,5	1,12	306,25	1,2544	19,6	15,0	1,1	225	1,21	16,5
3	19,2	1,27	368,64	1,6129	21,384	18,1	1,2	327,61	1,44	21,72
4	19,0	1,25	361,0	1,6625	23,75	18,5	1,2	342,25	1,44	22,2
5	20,0	1,29	400,0	1,6641	25,8	19,2	1,3	368,64	1,69	22,96
6	21,5	1,30	462,25	1,69	27,95	20,5	1,3	420,25	1,69	26,65
7	22,0	1,35	484,0	1,8225	29,7	24,6	1,35	605,16	1,8225	33,21
8	19,5	1,26	380,25	1,5876	24,57	19,0	1,12	361,0	1,2544	21,28
9	24,0	1,45	576,0	2,1025	34,8	23,7	1,45	561,69	2,1025	34,365
10	19,5	1,27	380,25	1,6129	24,765	19,0	1,3	361	1,69	24,7
∑	198,8	12,56	3994,2	15,9024	201,919	190,7	12,42	3744,28	15,5494	239,995
β	25,4					16,608				
R	0,94					0,86				
α	- 12,0224					- 0,9796				
Y=f(X)	P = - 12,02 + 25,4 I					P = - 0,98 + 16,6 I				

As a result of the experiments, the dependences Pотр= f(Iсв) and Pср= f(Iсв). were obtained. At the same time, the existence of a linear relationship between strength and welding current was assumed. In this case, the correlation

coefficient between the above parameters was adopted as a criterion for assessing the sensitivity of test schemes. We limited ourselves to consideration of the first order regression equation $Y=\alpha+\beta X$. The correlation coefficient r, the coefficients α and β were determined by the known formulas [37-39]:

$$\beta = \frac{m\sum X_i Y_i + \sum X_i \sum Y_i}{m\sum X_i^2 - \left(\sum X_i\right)^2};$$

$$\alpha = \frac{\sum Y_i - \beta \sum X_i}{m};$$

$$r = \beta \sqrt{\frac{m\sum X_i^2 - \left(\sum X_i\right)^2}{m\sum Y_i^2 - \left(\sum Y_i\right)^2}},$$

where the sample size is m=10.

The results of the experiment and calculation are presented in Table 1.1. In both cases of testing, a high correlation was found between the current and the force of separation and shear. However, some advantage can be given to the shear test, since in this case the correlation coefficient is greater (Fig. 1.4). This test scheme will be more sensitive to changes in the welding mode parameters, which is especially important when developing a mathematical model based on the welding mode parameters to assess the strength of welded joints.

Thus, to assess the strength characteristics of the quality of electrocontact welded joints of reinforcement, it is advisable to use the results of testing welded joints for shear.

In industrial and civil construction, in widespread structures made of unstressed reinforced concrete, class B-I, Bp-I reinforcement is used. It is a so-called. a metal mesh made of smooth wire with a diameter of 3-5 mm, which is made of low-carbon steel.

In meshes, metal wires are laid in two mutually perpendicular directions, and the places of their intersection are welded by the electrocontact method [40].

Factory-made metal meshes are shipped to enterprises manufacturing reinforced concrete structures in the form of rolls or in the form of flat pieces (Fig. 1.5).

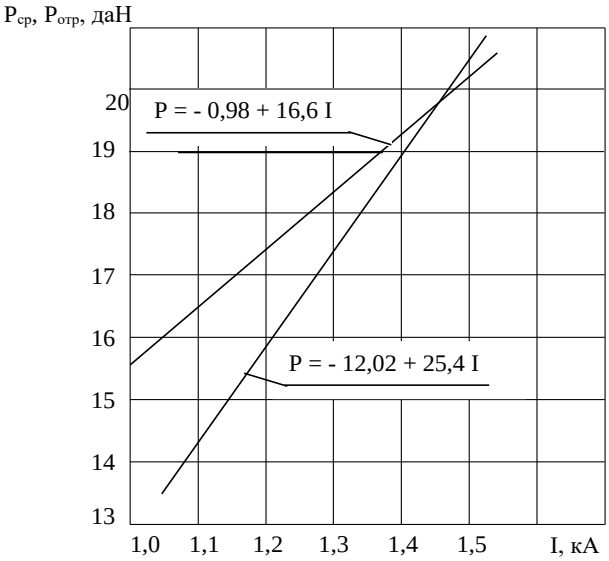

Figure 1.4. Dependences of strength on welding current for different schemes for testing welded joints.

Electrocontact welding of grids is carried out with one current pulse and with constant pressure on the electrodes at the welding site [2]. Accordingly, the main parameters of the welding mode are: welding current Iw, compression force Fw and welding duration tw.

For the production of metal meshes in production conditions, installations of multi-point electrocontact welding are used. In order to study the features of the development of energy-saving technology for the manufacture of metal meshes, we conducted experiments on the MT-75 machine for electric contact welding on the samples shown in Fig. 1.4.

In the experiment, the same values of the parameters of the welding mode Fco, tw were left unchanged, as in production conditions, and the welding current was changed in accordance with the data in Table 1.2. In experiments 6, 7, 8, the range of welding current variation corresponded to the current variation during mesh fabrication under production conditions. In other experiments, the decrease in the welding current was carried out by us gradually (experiments 1, 2, 3, 4, 5).

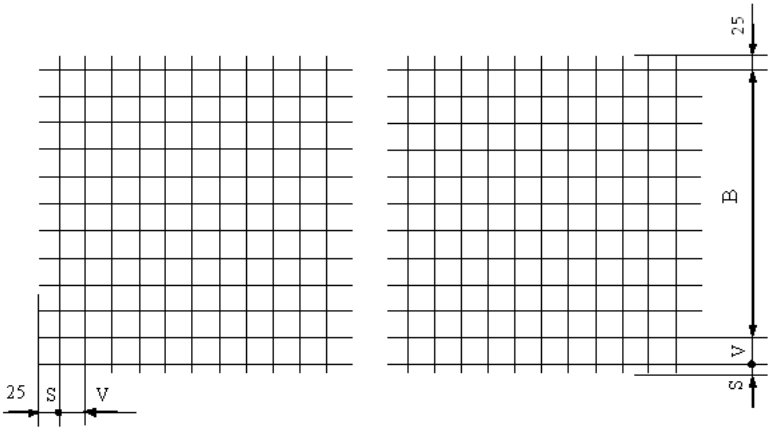

Figure 1.5. Welded metal mesh used in unstressed concrete structures.

In the rest of the experiments, the welding current was regulated by a stepwise change in the number of turns in the secondary winding of the welding transformer to regulate the secondary voltage. At each stage, the welding current was additionally regulated by introducing rings with ferromagnetic properties into the welding circuit. Welding modes and experimental results are given in Table 1.2.

In each welding mode, 10 samples were welded. During the experiment, in the process of obtaining each welded joint, the value of the welding current was determined, and its strength (P) was determined by mechanical testing of the corresponding welded sample. Based on their average values, a relationship was built between the strength of the welding spot and the welding current (Fig. 1.5).

On the basis of correlation studies, it was found that for the values of experiments 1, 2, 3, 4, 5, the correlation coefficient correlation and, accordingly, the segment of the IRR is non-linear. In this area, the strength dispersion of Sy is significantly reduced and it approaches the strength dispersion of mild steel.

Table 1.2. Welding modes, test results of welded joints

experience	sequence of experiments															
	1		2		3		4		5		6		7		8	
	X	Y	X	Y	X	Y	X	Y	X	Y	X	Y	X	Y	X	Y
1	0,6	8,5	1,0	13,5	1,2	17,6	1,6	23	1,9	29,2	2,4	35	4,0	33	4,0	33
2	0,8	11,0	0,9	13,5	1,07	18,5	1,6	23,6	1,9	29,6	2,4	35,5	3,9	33,8	3,9	33,8
3	0,5	10,0	1,1	14,0	1,0	19,0	1,58	24,5	1,95	30,5	2,4	34,5	3,9	33	3,9	33
4	0,5	8,5	1,15	14,5	1,0	20,0	1,6	25,5	1,82	29,2	2,35	35	4,0	33	4,0	33
5	0,7	9,0	1,0	15,5	1,2	20,0	1,8	24,0	1,83	29,8	2,35	35	3,9	33	3,9	33
6	0,65	11,0	1,0	15,0	1,25	20,0	1,75	24,6	1,84	30,5	2,35	34,8	3,9	33,5	3,9	33,5
7	0,4	8,0	0,75	14,0	1,25	20,0	1,40	23,5	2,05	29,5	2,3	35,2	4,1	32,8	4,1	32,8
8	0,5	9,5	0,65	14,5	1,40	19,5	1,35	24,5	2,07	29,8	2,3	36	4,1	32,7	4,1	32,7
9	0,6	9,5	0,75	15,0	1,25	19,0	1,45	24,5	2,07	30,2	2,3	35,5	4,1	32,7	4,1	32,7
10	0,7	10,5	0,9	16,0	1,2	19,0	1,42	25,3	2,1	29,5	2,35	36	4,1	33,0	4,1	33,0
$1/n\sum X_i$	0,595		0,92		1,182		1,555		1,953		2,12		3,2		4,0	
$1/n\sum Y_i$		9,55		14,65		19,26		24,30		29,78		34,03		35,25		32,99
S_Y		1,136		1,01		0,643		0,618		0,60		0,58		0,50		0,050
S_X	0,0147		0,026		0,0157		0,0601		0,06		0,058		0,055		0,05	

In the first case, in the heat-affected zone, plasticity decreases and brittleness increases, as a result of which, during mechanical action on the welding zone, the material being welded is destroyed in this zone, and not the welding site. This is also indicated by the fact that in the non-linear section, the strength of the welding spot depends slightly on the magnitude of the welding current and, accordingly, the non-linear section is falling.

In the second case, with an increase in current above 2.4 kA, the heat released in the welding zone increases, however, in accordance with this, the contact area of the parts to be welded does not increase, as a result of which the current density in the welding zone increases and because of this, a splash of molten metal takes place from the hot zone. On the other hand, the loss of energy as a result of splashes is the reason for the nonlinearity of the dependence. Despite this, with a change in the welding current in a large range (2.4-4.0 kA), the strength of the welding site changes relatively slightly (33-35 dan). Although, power losses are also significant.

If, when welding metal meshes manufactured at enterprises, the welding current is less than 2.4 kA, then the probability of obtaining a welded joint equal in strength to the base metal decreases and the possibility of obtaining welded joints with less than permissible strength is not ruled out. Therefore, it becomes necessary to control the quality of the strength of the welded joint in order to be able to timely correct the welding current in case of obtaining a welded joint with unacceptable strength.

Since the possibility of splashes during the welding process affects the strength of the welded joint and is associated with large energy losses, this phenomenon can be taken as an indicator of the quality of the welding process [41, 42].

CHAPTER 2. HEATING DURING RESISTANCE WELDING OF CROSSING ROUND RODS

In order to present a general picture of the process of welding crossed rods, experiments were carried out, as a result of which the change in temperature at various points of the welded joints and the settlement at the point of contact of the rods were established.

The experiments were carried out on mild steel, the chemical composition and mechanical properties of which are shown in Table 2.1.

Table 2.1. Chemical composition and mechanical properties of carbon steel

Chemical composition, %					Mechanical properties	
C	Mn	Si	S	P	Strength limit, dan/mm^2	Relative extension, %
0,24	0,45	0,02	0,031	0,045	47,0	37,0

Rods with a diameter of 5x10 mm were welded on an MT-65 machine in two modes:

- soft mode: welding current It=2100A;
  welding duration tsv = 8 sec;
  force on the electrodes 300 dan;
- hard mode: welding current It=2500A;
  welding duration tw = 3.5 sec;
  force on the electrodes 300 dan.

The temperature in the rods was measured with chromel-aluminum thermocouples with a wire diameter of 0.2 mm. The thermoelectromotive forces of the thermocouple were recorded on a loop oscilloscope.

The temperature was measured at three points. Of these, two points were located near the contact on the side of each rod being welded, and the third point was near the lower electrode (Fig. 2.1). Thermocouples were welded to the samples by capacitor welding.

The magnitude of the force on the electrodes was measured with a dynamometer using special devices.

The results of experiments when welding samples in a soft mode are shown in Figure 2.2.

The highest heating rate at the beginning of the process is observed at points located in the region of the welding contact (points 1, 2).

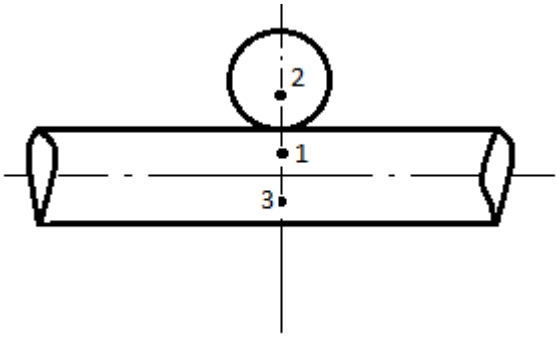

Figure 2.1. Location of points where the temperature was measured during welding

At a point located near the electrode (point 3 on the surface of the small rod), the heating rate is somewhat less.

Characteristic of this experiment is the formation of a platform of almost constant temperatures on the curves of the thermal cycle of those points that are in the region of the greatest heating of points 1,2. Obviously, at a certain stage of the welding process, in the area adjacent to the contact, thermal equilibrium sets in, in which the heat release due to the work of the current is balanced by the removal of heat due to thermal conductivity. The temperature of the points in this region hardly increases in the future [42–44].

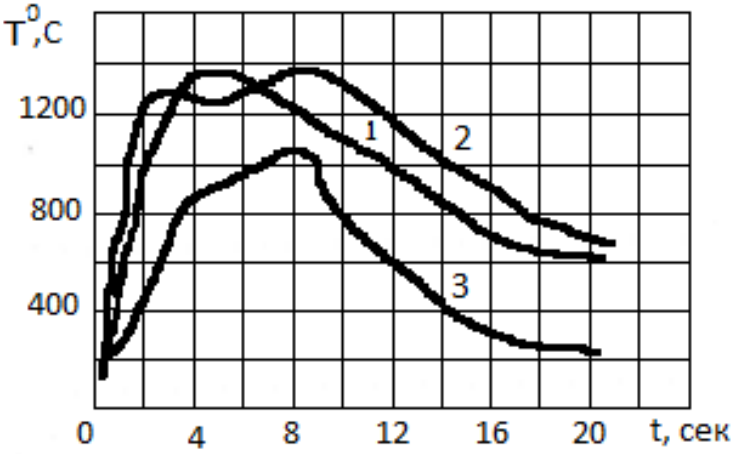

Figure 2.2. Thermal cycle of various points of the welded sample (soft welding mode)

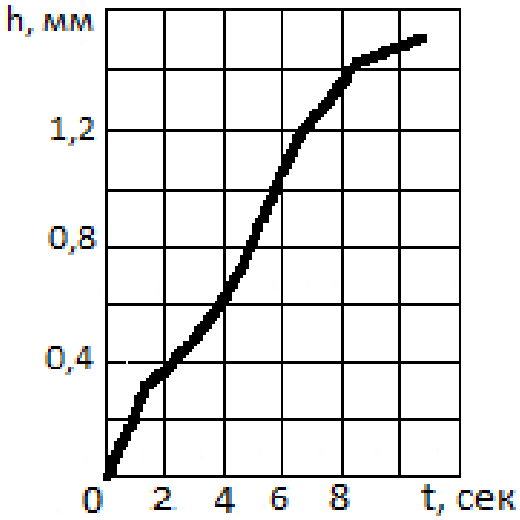

Figure 2.3. The dependence of precipitation on the duration of welding

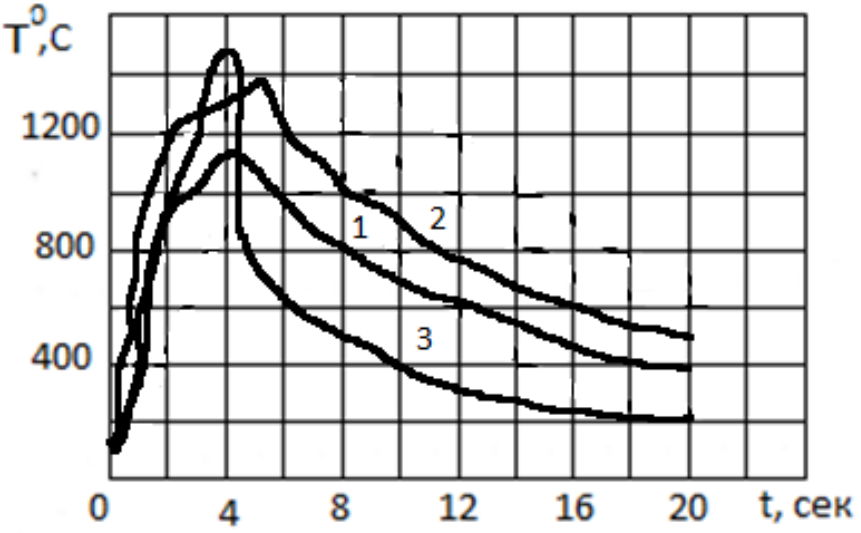

Figure 2.4. Thermal cycle of various points of the welded sample (hard welding mode)

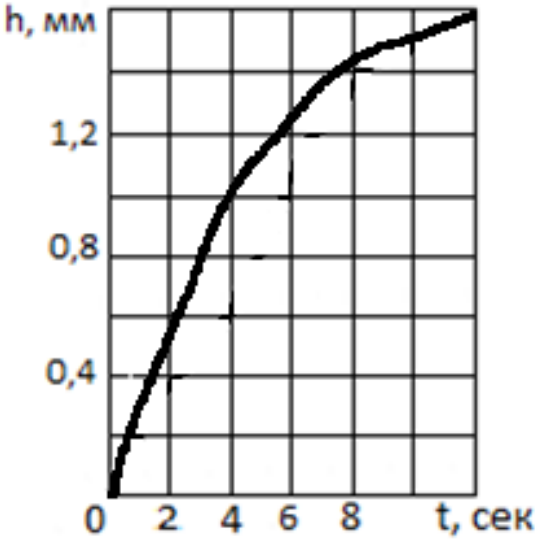

Figure 2.5. Dependence of the settlement between the rods on the duration of welding

With correctly selected mode parameters, in combination with the force on the electrodes, the steady state thermal state should correspond to the heating of the contact points to the melting temperature. Excessive force on the electrodes with insufficient current will reduce the current density in the welding contact, and the state of equilibrium will come before the necessary temperature is reached in the welding zone, which will lead to lack of fusion. Thus, the level of the equilibrium area on the thermal cycle curves is controlled by changing the electrical parameters in combination with the squeezing force [45-47].

The temperature of points 1, 2 reaches 1200-1400 A at the 2-5th second and remains almost constant until the current is turned off. Further release of thermal energy is spent on heating the points remote from the place of welding. By the time the current is turned off, the temperature at point 3 has time to rise to 1100-1150°C. The process of heating points near the electrodes also tends to a stationary state. However, the temperature at these points is only 500-600°C with the maximum steady-state temperature at point 1 equal to 1300°C. Therefore, the temperature of point 3, having somewhat slowed down the speed, continues to grow, reaching 250°C by the time the current is turned off.

As you can see, the duration of welding is 8 seconds. At a given current and force, squeezing leads to a strong overheating of the metal of a small diameter rod.

After the current is turned off, a period of cooling and temperature equalization begins. There are two stages of this period: 1) temperature

equalization with closed electrodes; 2) free temperature equalization and cooling with open electrodes [48-51].

The results of experiments during welding of samples in a hard mode are shown in Fig. 2.4.

Points close to the welding contact - points 1, 2 heat up at approximately the same rate as when welding in soft mode. This can be explained by the fact that a higher initial current density in the area of the welding contact caused a rapid increase in precipitation at the beginning of the heating process and, accordingly, a rapid decrease in the current density in the welding contact (Fig. 2.3, Fig. 2.5).

Thus, the near-contact region turned out to be heated to approximately the same temperature of the limiting state as in soft mode welding. The draft at this temperature during welding in a hard mode was 1.4-1.6 times higher (Fig. 2.5) than in the first case (Fig. 2.3). therefore, the heating of points remote from the contact, necessary to obtain the required draft, is achieved within 1.5-2 seconds, and when welding in a soft mode, the same amount of draft is achieved after 6-6.5 seconds. As a result of the reduction in the total duration of heating in comparison with the first experiment, the maximum temperature of the small rod, remote from the welding contact, turned out to be significantly lower in the second experiment.

The temperature equalization process can be considered completed 1.5-2 minutes after the start of the welding process. After this time, the temperature of all points of the large and small rods is between 150-200°C.

When a body is heated by a heat source of constant power, two stages of the process are distinguished: heat saturation and limit state. The closer the contact zone is to the heat source, the earlier the limit state occurs in it.

In resistance welding of crossed rods, heat sources are distributed over the volume of the metal and over the surface at the points of contact. Under the conditions of our experiments, the limiting state during welding was reached in the region adjacent to the welding contact.

For an approximate assessment of the nature of the process in this region, we use the calculation scheme of local heating by a spatially radial current of a massive body with a resistance that increases with temperature [52–55].

Let us represent the near-contact area of the crossed rods as a schematic semi-infinite heat-conducting body: the current J_2 is introduced into the body through the contact hemispherical cavity of radius r_0 and is distributed uniformly over its surface $2r_0^2$ [56–58].

Thus, the spatial-radial current density is calculated by the formula:

$$\gamma(r) = \frac{J}{2\delta r_0}^2.$$

If the initial temperature of the body is T (r, O) = 0, and the ratio of the resistivity of the metal ρom.cm to its volumetric heat capacity cγ (cal/cm3 deg) increases linearly with increasing temperature

$$\frac{\rho(T)}{c\gamma(T)} = \frac{\rho_0}{(c\gamma)_0}(1+\beta T). \quad (2.1)$$

Here ρ_0 and $(c\gamma)_0$ are the values of resistivity and volumetric heat capacity at zero temperature; β - temperature coefficient of increase in the ratio $\frac{\rho}{c\gamma}$1/deg.

The differential heating equation for a spatially radial process has the form:

$$\frac{\partial T}{\partial t} = a\left(\frac{\partial^2 T}{\partial r^2} + \frac{2\partial T}{r\partial r}\right) + 0{,}24\frac{J_2\rho_0}{4\pi^2\mu^4(c\gamma)_0}(1+\beta T), \quad (2.2)$$

where $a = \frac{\lambda}{c\gamma}$ - thermal diffusivity, cm^2/sec;

λ - thermal conductivity coefficient, cal/cm sec°C;
β - temperature coefficient, deg-1.
Let us introduce dimensionless process criteria:
$\theta = \beta T$ - relative temperature;

$\tau = \frac{dt}{\Gamma_0^2}$ - criterion of homochrony;

$\frac{\Gamma}{\Gamma_0} = \rho$ - relative radius;

$\mu^2 = \frac{0{,}24\beta\rho_0 I_2^2}{4\pi^2\alpha(C\gamma)_0\Gamma_0^2}$ - energy parameter characterizing the intensity of the heat source in the contact section of the heated body.

Equation (2.2) in dimensionless parameters will be written:

$$\frac{\partial\theta}{\partial\tau} = \frac{\partial^2\theta}{\partial\rho^2} + \frac{2}{\rho}\cdot\frac{\partial\theta}{\partial\rho} + \frac{\mu^2}{\rho^4}(1+\theta), \quad (2.3)$$

where $1 \le \rho \le \infty$; $0 \le \tau \le \infty$.

We accept the boundary conditions:
hemispherical boundary $r=r_0$ or $\rho=1$ impervious to heat

$$\frac{\partial\theta\rho}{\partial\rho_0^2}(1,\tau) = 0;$$

temperature and heat flow are equal to zero at $\rho=\infty$ at any time

$$\theta(\infty,\tau)=0,\quad \frac{\partial\theta}{\partial\rho}(\infty,\tau)=0;$$

At the beginning of the process, the temperature in the whole body is zero

$$\theta(\rho,0)=0.$$

Equation (2.3) is transformed by inversion of the spatially radial radius ρ.

This turns the semi-infinite region into a bounded one and makes it easier to solve the equation numerically

$$\vartheta=\frac{1}{\rho}=\frac{\Gamma_0}{\Gamma};\qquad 0\le\vartheta\le 1.$$

The process of heat saturation $\theta(\vartheta,\tau)$ obeys in the region, $0\le\vartheta\le 1$ $0\le\tau\le\infty$ the differential equation of heat conduction

$$\frac{\partial\theta}{\partial\tau}=\vartheta^2\left[\frac{\partial^2\theta}{\partial\vartheta^2}+\mu^2(1+\theta)\right] \tag{2.4}$$

under boundary conditions:

$$\frac{\partial\theta}{\partial\vartheta}(1,\tau)=0;$$

$$\theta(0,\tau)=0;$$

$$\theta(\vartheta,0)=0.$$

Equation (2.4) will be solved by the finite difference method. We divide the integration interval ϑ, which varies from 0 to 1, into n equal parts $\Delta\vartheta$, and the duration of the process - into K equal time intervals. We replace the derivatives entering equation (2.4) by the ratios of finite differences:

$$\frac{\partial\theta}{\partial I}\approx\frac{\Delta\theta_{К.П}}{\Delta I},$$

$$\frac{\Delta^2\theta_{К.П}}{\Delta\vartheta^2}=\frac{\theta_{К.ПН}+\theta_{К.П-1}-2\theta_{К.П}}{\vartheta^2}. \tag{2.5}$$

Equation (2.4) in finite differences takes the form:

$$\Delta\theta_{к.п} = \frac{\vartheta_п^4}{\Delta\vartheta^2}\left(\theta_{к,п+1} + \theta_{к,п-1} - 2\theta_{к.п}\right) + \vartheta_п^4\mu\Delta\tau(1+\theta_{к.п}). \quad (2.6)$$

Equation (2.6) expresses the temperature $\Delta\theta_{к.п}$ increment in the layer n, at time K, if the temperature of this layer $\theta_{к.п}$ and the two adjacent layers $\theta_{к,п+1}$ and $\theta_{к,п-1}$ is known. At the initial moment of the process, the temperature increment in all layers is due only to the presence of a term independent of temperature.

Assuming in equation (2.4) $\frac{\partial\theta}{\partial\tau} = 0$, we obtain the equation of the limiting stationary state of the process of heat propagation when the body is heated by a spatially radial current

$$\frac{\partial^2\theta_{ср}}{\partial\vartheta^2} + \mu^2(1+\theta_\infty) = 0, \quad (2.7)$$

whose solution under the following boundary conditions has the form:

$$\theta_\infty(1) = \theta_{max}; \quad \frac{\partial\theta_\infty}{\partial\vartheta}(1) = 0; \quad \theta_\infty(0) = 0; \quad \frac{\partial\theta_\infty}{\partial\vartheta}(0) = 0.$$

We get

$$\theta_\infty(\vartheta) = \frac{\cos[\mu(1-n)]}{\cos\mu} - 1. \quad (2.8)$$

The domain of existence of expression (2.8), i.e. the area of limitation of the limiting temperature $\theta_\infty(\vartheta)$, is determined by the condition cos μ>0. For cos μ=0, i.e. at μ= where m=0; one; 2; 3; …, the temperature increases indefinitely $\vartheta = 0$ everywhere except for.

The smallest critical $\mu = \frac{\tau}{2}$ value determines the current limit that causes an unlimited temperature rise.

Figure 2.6 shows a graph of the dependence of the limiting temperature $\theta_\infty(\vartheta)$ on the spatial coordinate for various values of the energy parameter μ characterizing the intensity of heat sources.

The process of heat saturation of the near-contact area is calculated by the finite difference method for the case of its heating by a heat source characterized

by a dimensionless parameter μ2=2 ($r = 1{,}41$, i.e. $\mu < \mu_{кр}$). The integration section was divided into 10 intervals $\Delta\vartheta = 0{,}1$.

To simplify calculations, Δτ was chosen from the condition

$$\frac{\Delta\tau}{\Delta\vartheta^2} = 1; \qquad \Delta\tau = \Delta\vartheta^2 = 0{,}01.$$

Newton's interpolation formula was taken as the condition on the boundary (in the 10th layer):

$$3\theta_{к,10} = 4\theta_{к,9} - \theta_{к,8} \ . \tag{2.9}$$

For 34 time intervals, the temperature was calculated with 10 layers; starting from $\tau = 0{,}34$, the number of layers was halved ($n = 5;\ \Delta\vartheta = 0{,}2$) and the time interval was correspondingly increased by a factor of 4 ($\Delta\tau = 0{,}04$).

The results of temperature calculation according to the formula (2.6) are presented by the graph in Fig. 2.7.

The temperature calculation by the finite difference method has not been brought to the limit state, because it can be assumed that the temperature in the contact is close to the limiting one and will be reached at $\tau = 400$.

Let us determine the ohmic resistance of a massive body with increasing resistivity when heated by a spatially radial current. The resistance dR of an elementary layer dr with a thickness at temperature is $T(r,t)$ expressed as

$$dR = \rho_0(1+\beta^2 T)\frac{dr}{2\sigma r^2} = \frac{\rho_0}{2\pi r_0}[1+\sigma\theta(\rho,\mu)]\frac{d\rho}{\infty^2} = \frac{\rho_0}{2\pi r_0}[1+\sigma\theta(\vartheta,\tau)]d\vartheta. \tag{2.10}$$

Here $\sigma = \beta^{\cdot}/\beta$ - is the ratio of temperature coefficients.

Since the dependence of resistivity ρ on temperature is assumed to be linear

$$\rho(T) = \rho_0(\mu + \beta^{\cdot} T),$$

with a temperature coefficient $\beta^{\cdot} = \sigma\beta$ exceeding the temperature coefficient β included in the linear dependence

$$\frac{\rho(T)}{c\gamma(T)} = \frac{\rho_0}{(c\gamma)_0}(1+\beta T)$$

Here ρ_0 and $(c\gamma)_0$ - the value of resistivity and volumetric heat capacity at zero temperature; β - temperature coefficient of ratio increase

$$\frac{\rho}{c\gamma}\frac{1}{\text{град}}$$

Integrating expression (2.10) over υ in the range from 0 to 1, we obtain the ohmic resistance of the body R:

$$R = \frac{\rho_0}{2\pi r_0}\int_0^1 [1+\sigma\theta(\vartheta,\tau)]\,d\vartheta\ . \qquad (2.11)$$

Cold resistance will be:

$$R_0 = \frac{\rho_0}{2\pi r_0}\ . \qquad (2.12)$$

Substituting the value $\theta_{\text{пр}}$ from (2.8) into expression (2.11), we obtain the resistance of the rod in the limit state:

$$R = \frac{\rho_0}{2\pi r_0}\left(\sigma\frac{t_g\mu}{\mu} - \sigma\right) + 1\ . \qquad (2.13)$$

The increase in the resistance of the body during heating to the limit state will be expressed at $\beta' = \beta$, i.e. with σ=1

$$\frac{R}{R_0} = \frac{t_g\mu}{\mu}\ . \qquad (2.14)$$

Figure 2.8. shows the dependence of the increase in resistance during heating to the limiting temperature for various values of μ. At $\mu = \frac{\pi}{2}$, the resistance increases indefinitely. An experimental study of the heating of crossed rods during resistance welding shows that the process reaches its limiting state in the area adjacent to the welding contact. For an approximate assessment of the nature of the heating process in this area, we use the calculation scheme expression (2.8).

We represent the near-contact region as a semi-infinite heat-removing body with a current source uniformly J_2 distributed over the surface of a hemispherical cavity of radius. The temperature of the limiting state of the point n of the near-contact region at time t for this case is determined by the expression:

$$\theta_{\infty}(t_{nt}) = \frac{cos[\mu(1-\vartheta_{nt})]}{cos\mu} - 1\,, \qquad (2.15)$$

where $\theta_{\infty} = \mu T_{\infty}$ - dimensionless temperature (T is absolute temperature °C);

β - temperature coefficient, deg-1;

$\vartheta_{nt} = \frac{r_{ot}}{r_{nt}}$ - inverted dimensionless distance parameter of point n at time t, located on the surface of a sphere of radius r_{nt} ;

$\mu = \frac{J_2}{2\pi r_{ot}}\sqrt{0{,}24\frac{\beta\rho_0}{\lambda}}$ - dimensionless parameter characterizing the intensity of heat sources;

ρ_0 - initial resistivity of the metal, Om cm;

λ - thermal conductivity coefficient at an average heating temperature of 500°C, (cal/cm)·sec·°C.

The parameter μ does not remain constant during the welding process, but changes as the current J_2 and r_{ot} radius of the contact hemisphere increase. At the beginning of the process, when r_{ot} small, μ has the greatest value, then quickly falls. The nature of the change in μ is due to the ratio of the electrical parameters of the regime and the compressive force. If the current load is such that for a given compression force μ reaches a critical value $\mu_{кр} = \frac{\pi}{2}$, then this means that the process has a limit state.

To obtain a high-quality welded joint, at the temperature $\theta_{\infty}(\vartheta_{nt})$ of the limiting state in the contact $\vartheta_{nt} - 1$ should not be lower than the melting point θ_{nt}, and heating should be stopped only after the necessary sedimentation of the rods occurs.

Having determined μ at one or another moment of the welding process, one can say whether the existence of a limit state is possible with such a ratio of mode parameters and what is the temperature of the limit state at various values of μ. The parameter μ can be determined if the welding current, the coefficients of the thermophysical properties of the welded material and the nature of the change in precipitation are known.

The temperature of the limiting state in the near-contact region is determined on the assumption that all previous heating occurs at a given value of μ. In fact, the process occurs at the beginning of the process at higher values of μ, and at the end of the process - at lower ones.

The relative distance of the point of interest to us also changes during the welding process:

$$\vartheta_{nt} = \frac{r_{ot}}{r_{nt}};$$

where r_{ot} - the radius of the contact hemisphere, increasing with the draft;

r_{nt} - the radius of the hemisphere on which the given point is located.

Below, for two typical modes, an example of calculating the limiting temperature of point N of a small core, located at a distance of 3 mm from the place of initial contact of the rods, i.e. from the surface of the rod, not yet deformed in the contact area.

When the rods are cold crumpled before the current is turned on, the projection area of the contact surface is about 4.6 mm^2, which corresponds to a draft of 0.07 mm. We calculate the distance of a point from the contact surface at any moment of the process as the difference between the distance of this point from the surface of the rod (3 mm) and the draft h_{ot} at this moment, i.e. $a_{nt} = (3 - h_{ot})$мм. The radius r_{nt} of the sphere on which point N is located,

we define, assuming that the distance from this sphere to the contact sphere at any time is equal to the experimental distance from the contact surface to point N (Fig. 2.9).

The results of calculating the parameter μ and the distance coordinate of the point N at various points in time are shown in Table 2.1.

The following thermophysical coefficients are taken into account:

$$\rho_0 = 13 \cdot 10^{-6}\,\text{Ом} \cdot \text{см};\ \beta = 0{,}5 \cdot \frac{10^{-3}1}{r};\ \gamma = \frac{0{,}1\text{кал}}{\text{см}} \cdot \text{сек}^0\text{C}.$$

Figure 2.10, 2.11 plot the experimental heating curve T_N of point N, show the curve of dependence of μ on the duration of welding t and the curve of limiting temperatures at this point, corresponding to the values of μ at any moment of the welding process. The intersection of the curves TN and Tpr determines the limit temperature of the point N (Tpr=13000), the moment of transition of the heat saturation process to the limit state (t=2 sec) and the value of μ at which the limit state μ=(1.45-1.46) occurs.

At the time t=1.5 sec μ reaches the critical value μcr=1.57 and then changes relatively little until the end of the process (from 1.57 to 1.04). The limiting temperature Tpr, calculated according to formula (2.15), drops from ∞ to 2000. A slight decrease in μ corresponds to a sharp drop in Tpr, therefore, the most favorable for obtaining the required temperature in the welding contact (Tpr> Tpl) is such a heating mode when μ is more for a long time remains above μcr and, if it reaches the value of μcr, then it decreases very slightly in the future, remaining greater than the value of μ, which corresponds to the limiting melting temperature Tmelt=Tmr.

At large μ, the required temperature in the contact can be reached faster than in the case of heating at small μ. The limiting state occurs at μ=1.45-1.46.

When welding in soft mode (Fig. 2.12, 2.13), the area of the weld spot at t=2 sec (25% of the total welding time) is 12 mm2, while when welding in hard mode t=2 sec is about 50% of the total duration welding, and the limit state occurs at the moment when the area of the weld spot reached 180 mm2.

Thus, the higher the current, the relatively later the limit state occurs, the shorter the duration of welding, and the less the possibility of overheating of the near-contact area.

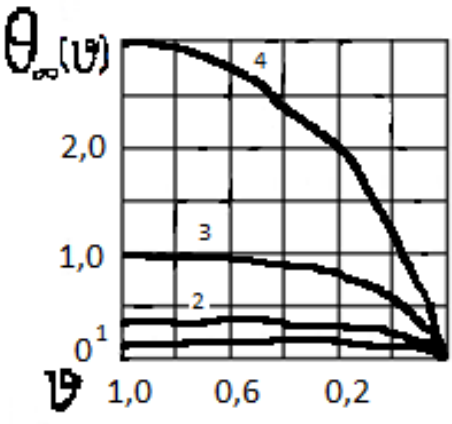

Fig. 2.6. Dependence of the limiting temperature $\Theta_\infty(\vartheta)$ on the spatial coordinate ϑ for different values of μ: $1-\frac{\pi}{6}2-\frac{\pi}{4};3-\frac{\pi}{3};4-\frac{5}{12}\pi$.;

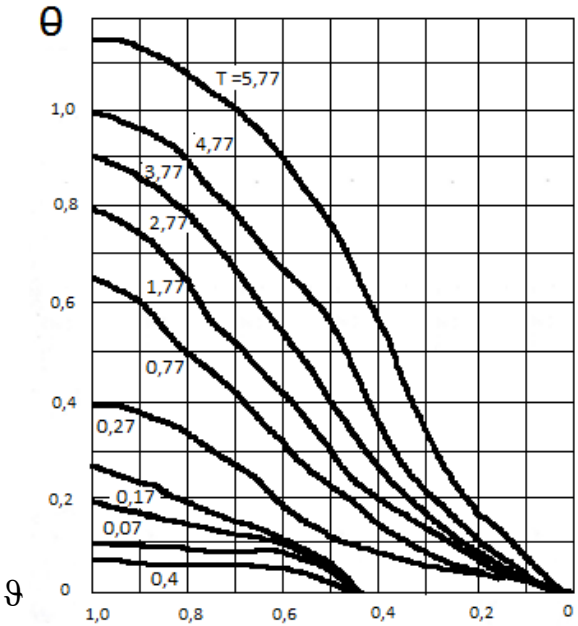

Fig. 2.7. Temperature curves $\Theta(\vartheta)$, obtained as a result of the calculation by the finite difference method of rods with increasing resistance

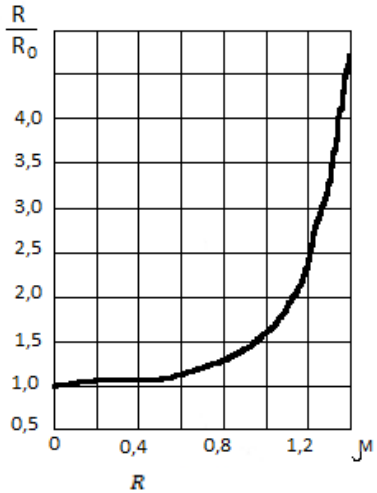

Fig. 2.8. Increase in the resistance $\frac{R}{R_0}$ of the near-contact region during heating to the limiting temperature at various values of μ.

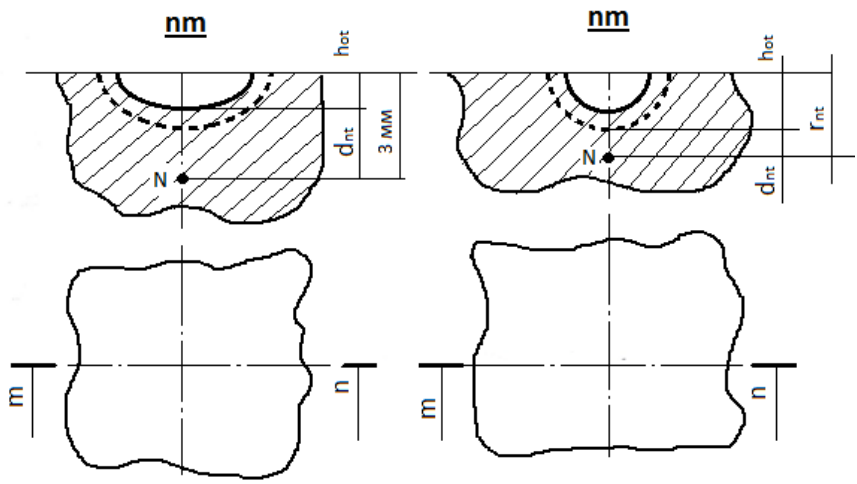

Fig. 2.9. To the calculation of the limiting temperature of the near-contact region.
a - contact area in the experiment; b - contact area in the design scheme.

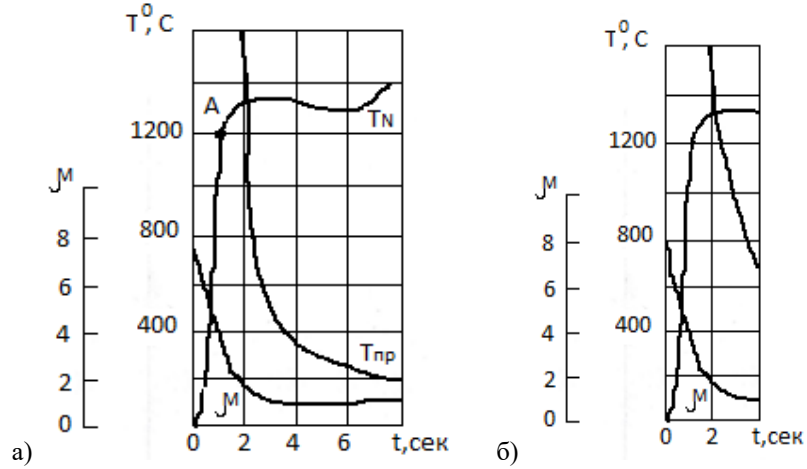

Fig. 2.10. Experimental heating curve T_N of the point N, to which the parameter μ corresponds, depending on the duration of welding t, limiting temperature $T_{пр} = \frac{1}{\beta}\left[\frac{cos\mu(1-\vartheta)}{cos\mu} - 1\right]$ the welding process corresponding to the values μ at any moment for two modes: a-soft; b-hard.

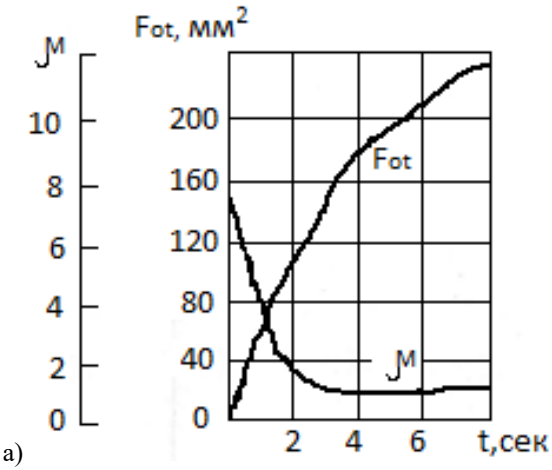

а)

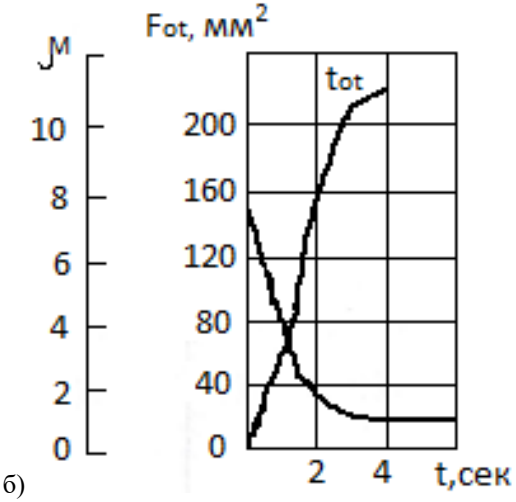

б)

Fig. 2.11. Parameter μ, characterizing the intensity of heat sources and the area of F_{ot} the contact hemisphere depending on the duration of welding t, for modes: a-soft; b-hard.

Table 2.2. The results of calculating the parameter μ and the distance coordinate υnt of the point N at different times

Time, t,sec	Current, I2, A	Draft, tot, cm	Projection area of the welding contact, Fot ,cm2	The area of the contact hemisphere $2Gr_{ot} = F_{ot}$		$\mu = \frac{I_2}{2\pi r_{ot}}\sqrt{0{,}24\frac{\beta\rho_0}{\lambda}} = 3{,}95 \cdot 10^{-6}$		The point N of the small rod at a distance of 0.3 cm from the initial contact		
				$\vartheta\, r_{ot}$, cm	F_{ot}, *cm*	$\frac{I_2}{2\pi r_{ot}}$	μ	$\propto_{Nt} = 0{,}3 - h_{ot}$, cm	$r_{Nt} = \propto_{Nt} + r_{ot}$, cm	$\vartheta_{Nt} = \frac{r_{ot}}{r_{Nt}}$
0	9500	0,007	0,046	0,0075	0,086	18000	1	0,293	0,380	0,229
1	10000	0,062	0,780	0,124	0,346	4600	1,82	0,238	0,584	0,594
2	10000	0,085	1,180	0,180	0,434	3680	1,45	0,217	0,649	0,670
3	10000	0,112	1,500	0,240	0,490	3260	1,29	0,188	0,678	0,724
4	10000	0,132	1,640	0,262	0,512	3100	1,22	0,168	0,680	0,754
5	10000	0,154	1,820	0,290	0,539	2960	1,17	0,146	0,685	0,800
6	10000	0,182	1,980	0,316	0,563	2840	1,12	0,118	0,681	0,825
7	10300	0,207	2,120	0,338	0,580	2770	1,09	0,093	0,673	0,863
8	10400	0,237	2,280	0,364	0,604	2750	1,08	0,063	0,667	0,905
0	11300	0,007	0,046	0,0075	0,086	21000	8,30	0,293	0,380	0,229
1	12500	0,097	1,340	0,213	0,461	4320	1,71	0,203	0,664	0,694
2	12500	0,155	1,820	0,290	0,539	3700	1,46	0,145	0,684	0,778
3	12700	0,190	0,020	0,323	0,569	3550	1,40	0,110	0,679	0,839
4	12900	0,219	2,200	0,350	0,592	3470	1,37	0,081	0,637	0,880

CHAPTER 3. QUESTIONS OF THE DEVELOPMENT OF RATIONAL TECHNOLOGY OF RESISTANCE WELDING OF REINFORCED CONCRETE REINFORCEMENT

In resistance welding of reinforced concrete reinforcement, the welded rods are compressed between the electrodes of the contact machine so that the centers of the contact pads are located at the ends of the same rod diameter (Fig. 3.1).

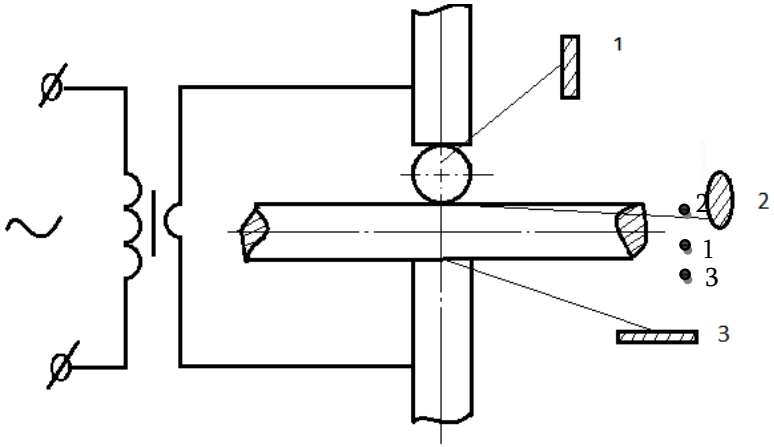

Fig. 3.1. Scheme of resistance welding of crossed rods and outlines of contour areas: 1, 3 - between the electrode and the rod; 2 - between the rods.

Schematizing the process of resistance electric welding of crossed rods, it can be represented as a set of simultaneously occurring and continuously interacting processes [59-63], the main of which are: a) plastic deformation of the metal in the welding zone of the rods (deposit); b) current distribution in the rods; c) distribution of heat sources; d) temperature distribution.

These processes are well known for resistance welding of crossed steel bars of large diameter (greater than 16 mm).

In connection with the expansion of the field of application of reinforced concrete structures in the national economy, much attention has been paid in recent years to the development of a rational technology for resistance welding of reinforced concrete reinforcement with a diameter of about 10 mm, especially resistance welding of a metal mesh from repainting round rods with both the same and different diameters.

Consider the process of electric contact welding of crossed round rods with diameters of 10 + 5 mm.

The dimensions and outlines of the contact pads depend on the shape and dimensions of the rods to be welded and current-carrying electrodes, as well as on the

compressive force applied to the electrodes [64-67]. The outline of the working contact pad between intersecting round rods of the same diameter is almost close to a circle.

As the diameter of one of the intersecting rods increases, the working pad extends along the generatrix of the small rod and along the circumference of the large rod. A conductive contact pad between a copper electrode with a flat surface and a round steel rod [68, 69] is located along the strip along the generatrix of the rod (Fig. 3.1).

Industrial frequency current, heating rod, distributed over the volume of the rod between the contact pads - conductive and working, i.e. directed parallel to the diameter of the rod, in what follows we will call such a current transverse (with respect to the axis of the rod).

We will calculate the distribution of the transverse current in a round rod based on the following assumptions:

A round conductive cylinder of radius ro (cm), with the Oz axis (Fig. 3.2) is considered to be infinitely long, which corresponds to the practical conditions for welding reinforcing bars.

The conductivity σ (ohm-1·cm-1) of the material is assumed to be constant in the entire volume of the cylinder. This assumption corresponds to a cold rod, i.e. state at the beginning of the heating process.

The transverse current Ja is considered constant, i.e. the influence of the industrial frequency of the current on its distribution is neglected. This assumption is supported by high current densities during resistance welding in the central zone of the rod between the contacts.

We consider the current to be applied to the cylinder through strip contact pads 1 and 2 on its side surface, the centers of which are located on the axis of the OS. The sizes of contact pads 1 and 2 are assumed to be different, namely in the direction of the generatrix of the cylinder: 2Z1 and 2Z2, and in the direction of the circle - 2φ1r0 and 2φ2r0. Such a rather general assumption covers various types of pad outlines encountered in practice. In reality, the outlines of the working contact areas are more or less rounded; if we take the outline of the pads as a strip, then this will distort the current distribution mainly at the corners of the rectangular pad, and even more so, the closer the outline of the site is to a square.

The current J is distributed evenly over the surface of contact pads 1 and 2, so the radial current densities are expressed as:

$$j_1 = \frac{I}{4Z_1\varphi_1 r_0} \quad \text{and} \quad j_2 = \frac{I}{4Z_2\varphi_2 r_0} \; . \tag{3.1}$$

The conditions for the distribution of current or potential over the area of the working or conductive contact are difficult to determine and they depend on the size and shape of the rods and electrodes. The simplest assumption that we have adopted about the constancy of the current density over constant areas is also

justified by the fact that the increase in current density at the edges of the contact area in a cold massive body quickly equalizes due to local overheating of this zone by a current of increased density.

Outside the contact pads, the side surface of the rod is considered isolated [70–72].

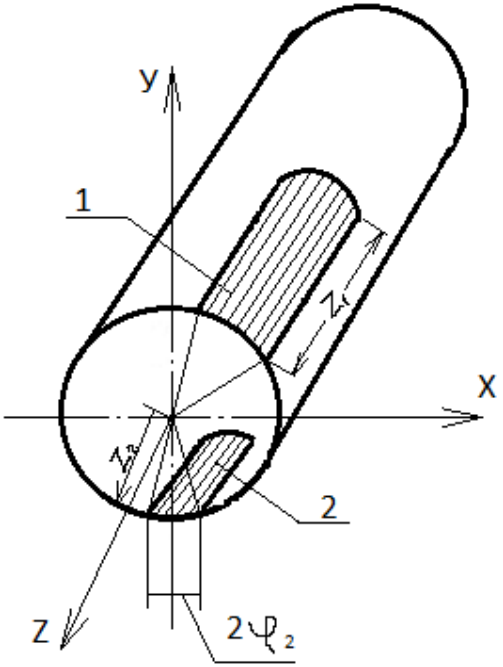

Fig. 3.2. Scheme of contact pads in a conductive rod

During contact welding of crossed round rods, elastic-plastic deformation of the metal occurs in zones remote from the contact, and plastic deformation occurs at the points of contact. The most interesting in studying the process of formation of a weld spot is plastic deformation in a welding contact [73-75].

Even before welding, a cold contact area appears between the rods as a result of their preliminary crushing. The horizontal projection area F of the crumpling surface is determined by the force P applied from the side of the electrodes and the specific crumpling pressure K.

At the beginning of heating, the contact area between the rods is small. The increased current density in the contact and the high contact resistance contribute to the intense release of heat at the point of contact between the rods. The contact resistance drops sharply, however, heat continues to be released mainly in the

contact zone due to the work of the current on the increased resistance of the heated metal. The intensity of the volumetric heat sources due to the work of the current on the metal's own resistance increases, while the intensity of the surface heat source in the contact decreases.

With an increase in the temperature of the near-contact region, the resistance to crushing decreases, and the contact area under the action of the force P increases. As the rods settle and the contact area increases, the average current density in the contact decreases, and the streamlines are pushed to the expanding boundaries of the contact surface.

The distribution of heat sources, their intensity and duration of action directly affect the temperature distribution in the rods at one or another moment of the welding process [56, 57].

Thus, the draft of the rods, the distribution of current and temperature are inextricably linked, continuously changing during the welding process, influencing each other.

The problem of plastic deformation in resistance welding of crossed rods can be classified as a die indentation problem, which is considered in the theory of plasticity. However, when solving these problems, the researchers limited themselves to the condition that a rigid stamp is pressed into a plastic medium. The task becomes much more complicated if we assume that the stamp itself is deformed during extrusion.

Our task is all the more difficult because heating occurs in the contact zone, which is non-uniform in space and variable in time. At present, there is no theoretical solution to this problem; therefore, the relationship of individual parameters that interests us in the process of crimping the rods was established empirically.

When studying the nature of the distribution of heat sources, it is necessary to know the dimensions of the contact areas, the direct determination of which at one time or another of the welding process is very difficult due to the extrusion of the heated metal from the welding zone. Therefore, we have established an approximate relationship between the contact area and the amount of settlement (mutual penetration) of the rods. The draft is such a parameter that is convenient to change during the welding process.

The relationship between the draft and the contact area was studied beforehand when cold rods were crushed.

Round rods 5 + 10 mm in diameter, machined from mild steel, were compressed in the direction perpendicular to the axes of the rods, on a shopper press, using special mandrels in which the rods were superimposed one on top of the other at an angle of 900 to each other. As a result of deformation, a saddle-shaped surface was formed at the point of contact between the rods.

The relationship between the draft and the contact area was studied beforehand when cold rods were crushed.

Round rods 5 + 10 mm in diameter, machined from mild steel, were compressed in the direction perpendicular to the axes of the rods, on a shopper press, using special mandrels in which the rods were superimposed one on top of the other at an angle of 900 to each other. As a result of deformation, a saddle-shaped surface was formed at the point of contact between the rods.

$$F = \frac{\pi d^2}{4}.$$

Fig. 3.3 shows the dependence of the diameter d of the projection of the contact print on the value of the draft h, obtained by calculation according to the scheme, i.e. between d and h there is the following relationship

$$d = 2\sqrt{2hR - h^2},$$

where R - cylinder radius.

Experimental points are plotted on the same graph according to Table 3.1. Experimental points are located near the calculated curve. This indicates that there is a certain relationship between the draft and the dimensions of the contact area, which is the same for metals with different ductility. This ratio is close to the ratio of geometric elements of intersecting cylinder curves.

Table 3.1. Results of experiments on cold bending of crossed rods with diameters of 16+16 mm.

Sample material	Crushing force P, dan	Contact imprint projection diameter between rods d, mm	Specific bearing pressure in contact K, dan/mm2	Settlement between rods h, mm
Steel HB146,6	1100	3,8	97,0	0,30
	2100	5,4	92,0	0,50
	3120	6,5	95,0	0,60
	4150	7,7	94,0	0,80

Figure 3.3 shows the dependence of the projection area of the contact surface on the force compressing the rods. The specific pressure K in the contact, which represents the ratio of the force P to the projection area of the contact surface, is constant, and for a given combination of diameters it has a quite definite value. For diameters 16 + 16 mm, the specific pressure, as can be seen from table 3.1, is about 0.6 Brinell hardness numbers for this material:

$$K \approx 0{,}6HB;$$

Cold bending experiments were also carried out on mild steel rods (St.3) with diameters of 16+30 mm and 5+10 mm. The horizontal projection of a saddle-shaped imprint in contact approaches an ellipse with semi-axes a and b. Table 3.2 and Table 3.3 show the dimensions a and in the projection of the contact print and the deposit h, obtained by squeezing the rod with different force P. The area F of the projection of the contact surface is calculated as the area of the ellipse with semiaxes a and b

$$F = \pi \cdot a \cdot b,$$

a - specific pressure

$$\text{K} = \frac{\text{P}}{F}.$$

Table 3.2. Results of experiments on cold bending of crossed rods with unequal diameters of 16 + 30 mm.

Sample material	Crushing force P, dan	Rod draft h, mm	Contact projection area F, mm2	Specific pressure K, dan/mm2
Steel HB146,6	1010	0,20	12,4	81
	2700	0,43	34,7	78
	3700	0,59	48,0	77
	4900	0,74	61,7	79
	6600	1,25	87,0	76
	7700	1,75	100,0	77
	10000	2,15	129,5	77

Table 3.3. Results of experiments on cold bending of rods with small diameters of 5 + 10 mm.

Sample material	Crushing force P, dan	Rod draft h, mm	Contact projection area F, mm2	Specific pressure K, dan/mm2
Steel HB146,6	200	0,20	6,01	128
	400	0,27	10,07	126
	800	0,40	12,18	127
	1000	0,80	14,17	128
	1200	1,00	18,07	128

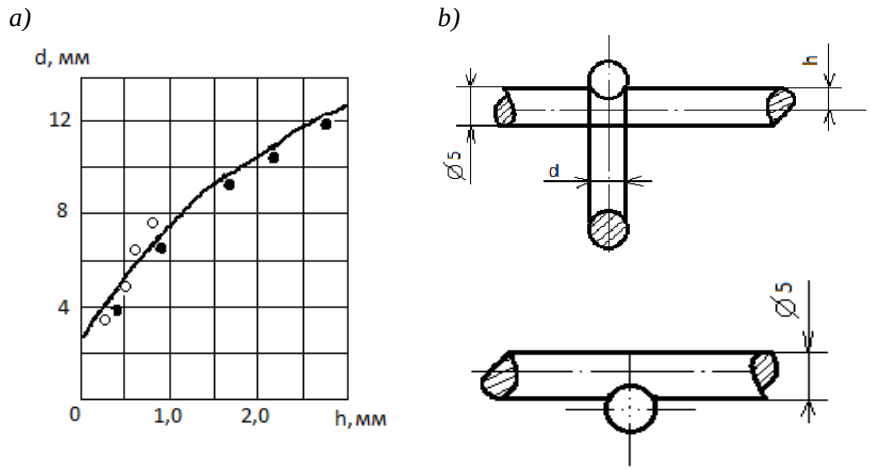

Fig. 3.3. Diameter d of the projection of the contact print depending on the amount of draft h during cold bending of rods with diameters of 5 + 5 mm (a) and samples after cold bending (b).

The area of the contact surface between the rods for a given draft can be calculated with sufficient accuracy by the ratio of the geometric elements of intersecting round cylinders of the same diameter (Fig. 3.4).

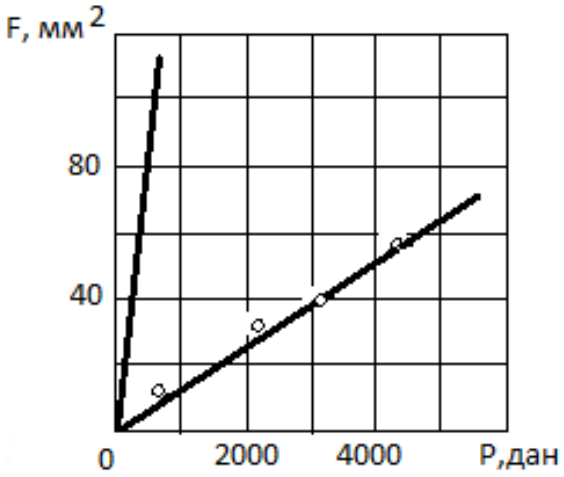

Fig. 3.4. The area F of the projection of the contact imprint, depending on the force P, compressing the crossed rods with a diameter of 5+5 mm during cold crimping.

The established relationship between the upset and the dimensions of the contact surface does not apply, however, to the deformation of the rods during welding, when the plastic properties, due to uneven heating of the metal, change sharply in the direction of the compressive force.

The conditions for plastic deformation of rods during welding are important from the conditions of deformation of homogeneous rods with significant volumes by volume. Significant specific pressure at the beginning of the rebellion against a sharp increase in spread due to the detection of fine heated metal. In this case, the colder metal surrounding the heated surface is subjected to the free age of precipitation. This is the result of natural development between sediment and vaccine. The area of infection with subsequent precipitation increased as a result of cold rods more resistant than in fainting.

Four batches of samples from low-carbon steel (St.3) with diameters of 5 + 10 mm were welded on the MT-75 resistance spot welding machine with current I_2=2100 *A* for 2 sec (I batch), 4 sec (II batch), 6 sec (III batch), 8 sec (IV party). The force on the electrodes of the machine was kept constant during the welding process and amounted to approximately 300 dan. Welded samples were destroyed at the place of welding. According to the measured semi-axes a and b, the area Fwel Fsv of the ellipse was determined, which is a horizontal projection of the contact surface

$$F_{св} = \pi \cdot a \cdot в.$$

Figure 3.5 shows the dependence of the dimensions of the contact surface on the duration of heating t.

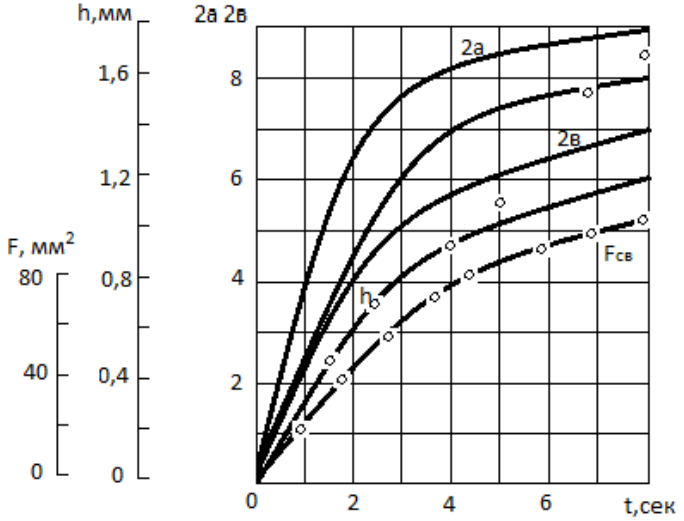

Fig. 3.5. Dimensions of the welding contact depending on long-term heating during welding of rods Ø5 10 mm, current I_2=2100 *A* at a compressive force P=300 dan.

Another batch of samples was welded with the same current for 8 seconds and the change in precipitation was monitored. The graph of changes in draft h in time *t* is also shown in Fig. 3.5. From the comparison of curves $F_{CB}(t)$ and $h(t)$ obtained dependence of the area of the projections of the contact on the draft $F_{CB}(h)$, presented in Fig.3.6. The same figure shows the dependence $F_x(t)$ of the cold contact projection area on the upset, obtained from experiments on cold bending of a rod of the same diameter and coinciding with the calculated dependence for geometric bodies.

From comparison $F_{CB}(h)$ and $F_x(h)$ follows that $F_{CB}(h) \approx 1{,}8F_x(h)$.

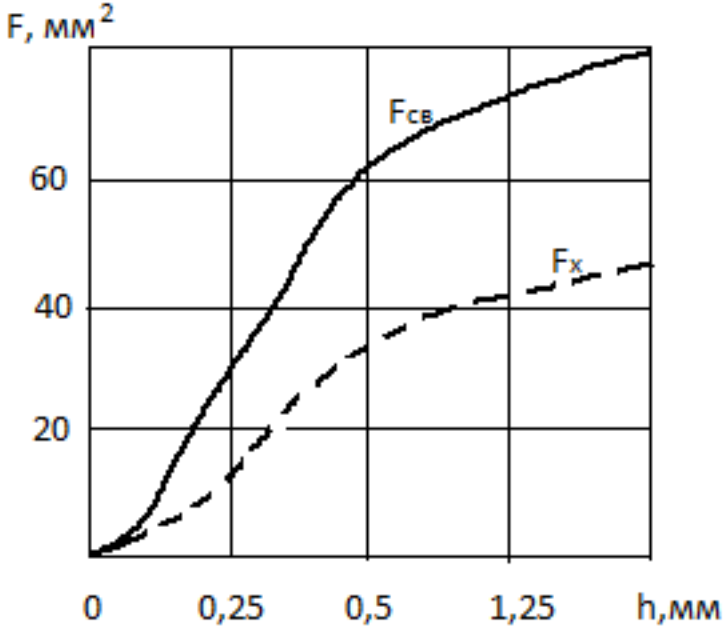

Fig. 3.6. The projection area of the contact between the rods depending on the draft during welding $F_{CB}(h)$ and during cold bending of the rods $F_x(h)$.

The nature of the upsetting process during welding in two typical modes

А) $I_2 = 2100$ А; $t_{св} = 8$ сек; (soft mode);

Б) $I_2 = 2500$ А; $t_{св} = 3{,}5$ сек; (hard mode),

studied on samples of mild steel (St.3) with a diameter of 5 + 10 mm. The samples were welded on an MT-75 machine with long-term compression between the electrodes of the machine after the current was turned off. The force on the electrodes of the machine was 300 dan.

Figure 3.7 shows a graph of changes in settlement and the average value for each group of experiments. A less intense growth of precipitation is observed when welding in a soft mode (A). For 8 seconds of the welding process, the deposit increases to 1.5 mm. In samples welded in mode B, the sediment reaches approximately the same value in 3.5 seconds.

Thus, the average upsetting rate over the welding time is 0.25 mm/sec when welding in soft mode A, and 0.57 mm/sec when welding in hard mode B.

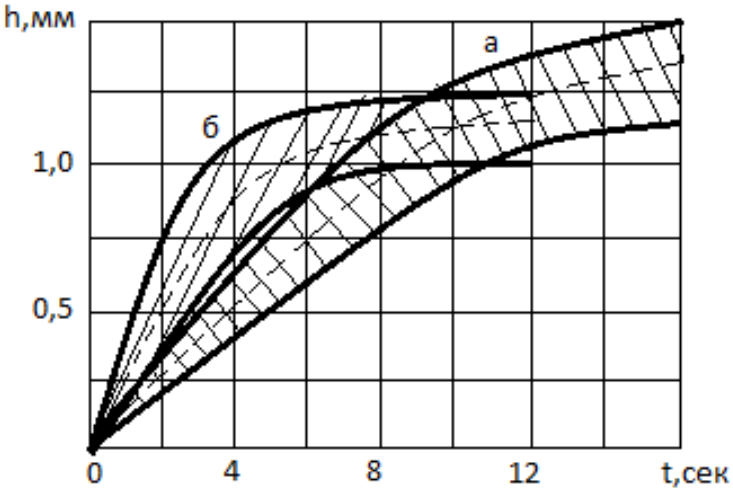

Fig. 3.7. Change in rod settlement during welding: a - mode A, b - mode B; - - - - average value of draft.

After the current is turned off, under the action of force P, the precipitation continues to grow, and a longer, although less intense, growth of the precipitation is observed in rods welded in a softer mode. In specimens welded in a hard mode, the rate of upsetting growth decreases significantly already 1–1.5 sec after the current is turned off, and after 5–6 sec, plastic deformation in the welding contact zone practically stops. Apparently, when welding in a soft mode in the welding zone, the amount of molten metal is greater, respectively, the volume of extruded metal is greater. This is confirmed by external inspection of welded joints.

Thus, when welding in a soft mode, part of the electricity spent on heating the welding zone is not spent for the formation of a welded joint. Therefore, in order to save energy, it is advisable to carry out electric contact welding of crossed rods in a hard mode.

In another series of experiments, in addition to upsetting, the welding current and temperature were measured and recorded at individual points of the welded sample during the welding process.

According to the average settlement, in these experiments, the projection area of the welding contact was obtained. The average draft h and the average area are plotted on graphs (Fig. 3.8), from which it can be seen that at the end of the welding process, at the moment the current is turned off, the area of the weld spot is the maximum value. The specific pressure at the point of contact of the rods at this moment is 1.5-1.6 dan/mm2. In the future, the specific pressure decreases somewhat due to an increase in the size of the contact area of the rods, and the yield strength of the near-contact zone, as the temperature cools and equalizes, decreases, i.e. conditions for the further development of precipitation become less and less favorable.

Figure 3.7 also shows the average current and the average current density in the contact for any moment of time, obtained by dividing the current by the projection area of the contact *Fx* corresponding to a given moment of the welding process. A particularly sharp change in current density occurs at the beginning of the process, during the first second.

Despite some increase in current in the first second of the process, when welding in soft mode, the current density in the welding contact drops by almost 10 times (Fig. 3.9). Then the current density changes more slowly, reaching 55 A/mm2 by the end of the welding process. The current density drops even more sharply in the initial stage of the process when welding in a hard mode. During the first second of the welding process, the current density in the welding contact drops by almost 20 times.

In accordance with the current density, heat sources change and redistribute. The heat sources are redistributed most sharply at the beginning of the process. Figure 3.10 shows the change in the specific pressure in the welding contact depending on the duration of welding, and Figure 3.11 shows the dependence of the upsetting rate dh / dt on the specific pressure in the contact K. When welding in a softer mode, the highest upsetting rate is 0.6 mm/sec is observed at the beginning of the process at a maximum specific pressure in the contact of about 70 dan/mm2.

After 1-1.5 seconds after the start of the process, the pressure decreases to 5 dan/mm2 and the deposit from this moment increases until the end of the welding process at an almost constant speed of 0.2 mm/sec. By the time the current is turned off, the pressure in the contact is 1.5 dan/mm2. The upsetting rate drops sharply after turning off the current, and at K=1.4 dan/mm2, the upsetting practically stops ($\frac{dh}{dt} = 0$).

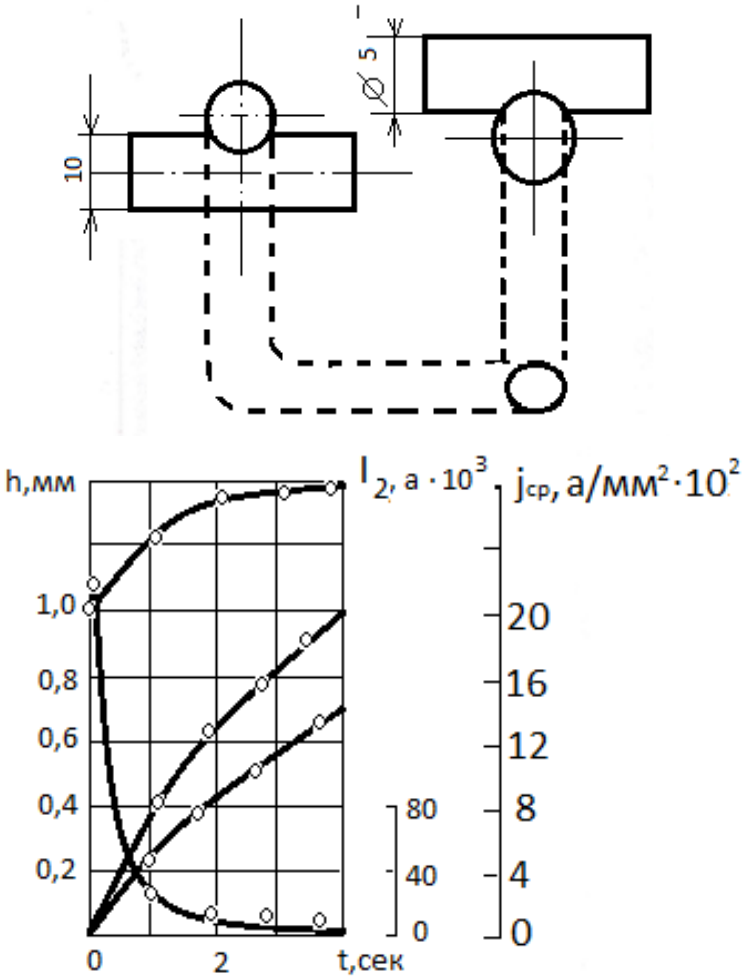

Fig. 3.8. The change in current, precipitation h between the rods, the area of the welding contact and the average current j_{cp} density in the contact during welding at P=300 dan is given for rods with a diameter of 5+10 mm in a hard mode.

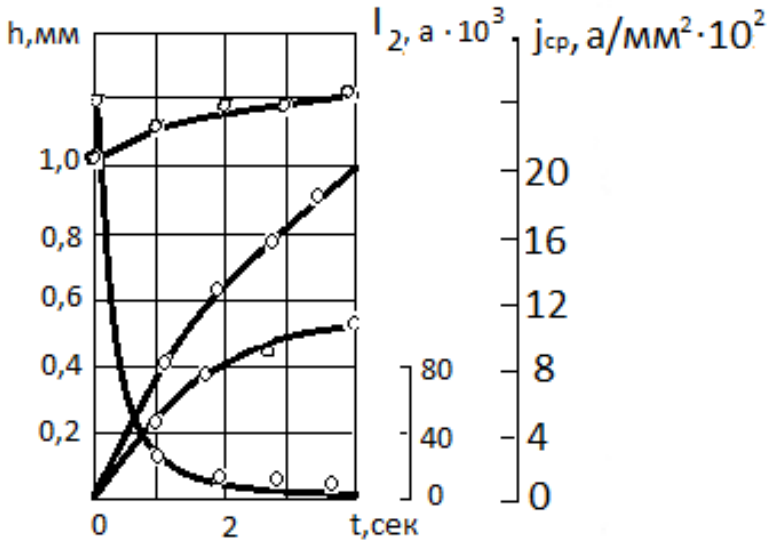

Fig. 3.9. The change in current I_2, precipitation h between the rods, the area of the welding contact F_{CB} and the average current j_{cp} density in the contact during welding at P=300 dan is given for rods with a diameter of 5+10 mm in soft mode.

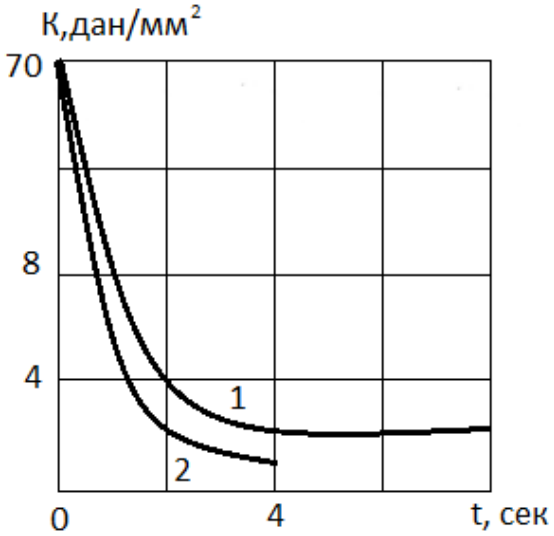

Fig. 3.10. Change in specific pressure K in the welding contact depending on the welding time t: 1 - soft mode; 2 - hard mode.

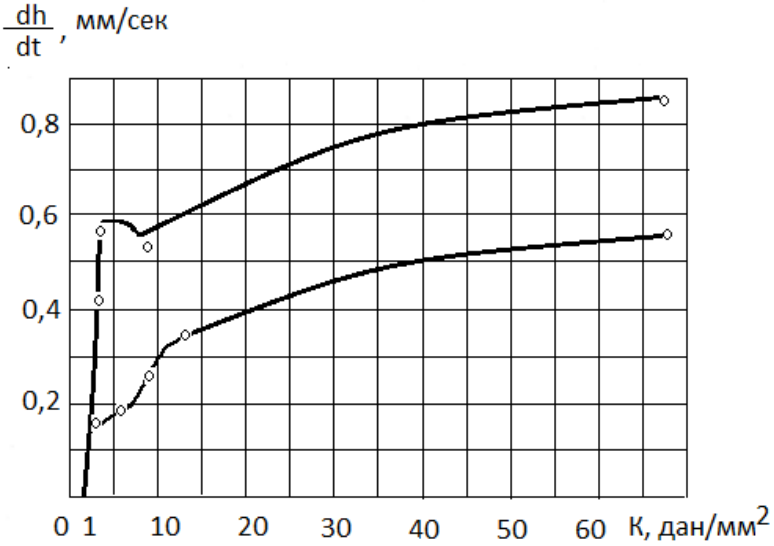

Fig.3.11. The upsetting rate dh/dt of the rods depending on the specific pressure K in the contact: - - upsetting speed with current; - - - - precipitation rate without current; lower curve – soft mode; upper curve - hard mode.

When welding in a hard mode, the upsetting rate is greatest at the beginning of the process, and decreases during the entire welding process. At a pressure in the welding contact of about 2.5 dan/mm2, even before the current is turned off, a sharp decrease in the upsetting rate from 0.5 to 0.3 mm/s occurs. The specific pressure in the welding contact at the moment of switching off the current is about 1.5 dan/mm2. After turning off the current, the precipitation continues for 5-6 seconds, however, the precipitation rate is so low that the pressure in the contact practically does not decrease. For further upset growth, efforts are required that are greater than for upsetting of specimens welded in a softer mode [76–78].

If we assume that the effective power of heat sources in electric contact welding does not change during heating, then it can be determined by the heat content of the welded sample by the time the current is turned off

$$q_{\text{ср}} = \frac{\theta_{\text{обр}}}{t_{\text{св}}},$$

sample heat content

$$\theta_{\text{обр}} = \eta_{\text{н}} 0{,}24\, U_{\text{н}} I_2 t_{\text{св}} \cos\varphi_{\text{н}},$$

where U_H - voltage at the welding section of the secondary purpose of the welding transformer;

I_2 - welding current;

η_H - effective efficiency heating process;

φ_H - phase angle between current and voltage at the welding section of the secondary circuit.

Effective efficiency the heating η_H process can be determined empirically by measuring the heat content $\Theta_{обр}$ of the sample in a water calorimeter and comparing it with the total amount of heat $0{,}24\ U_н I_2 t_{св} cos\varphi_н$, calculated from the electrical parameters of the welding mode:

$$\eta_н = \frac{\theta_{обр}}{0{,}24\ U_н I_2\ t_{св} cos\varphi_н}.$$

According to the author [65], the heat content $\Theta_{обр}$ of samples and electrodes was determined by calorimetric experiments $\Theta_{эл}$ depending on the duration of welding at two current values: at current $I_{2ср}$=10600 *A*, the duration of welding varied from 2 to 8 sec; at current $I_{2ср}$=12900 *A*, the duration of welding varied from 1 to 4 sec, after 1 sec. The experiments were carried out on samples made of rods with diameters of 30+16 mm.

In the experiments, the electrodes were not cooled by water during the welding process, so all the heat removed under normal welding conditions by the cooling water was absorbed by the electrodes and transferred to the calorimeter. During the welding process, the welding current was measured I_2, the voltage drop between the working surfaces of the electrodes, U_H and U'_H the voltage drop in the secondary circuit section, including the samples and electrodes.

As a result of the analysis of experimental data, Figs. 3.12, 3.13, 3.14, 3.15.

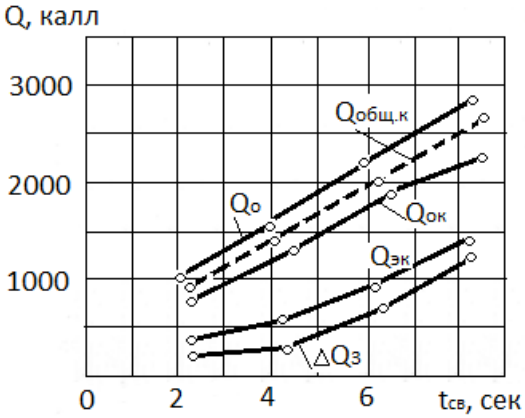

Fig. 3.12. The dependence of the heat content of samples and electrodes on the duration of heating by current at I_2 = 10600A, U_H = 1.57 V, P = 300 dan. $Q_{ок}$ - heat content of the sample; $Q_{эк}$ - heat content of electrodes (soft welding mode).

In Fig.3.12 and Fig.3.14, the solid lines show the heat content obtained from the experiment, and the dotted lines show the heat calculated from the electrical parameter of the welding mode.

The designations in the Picture are as follows:

$Q_{ок}$ - the heat content of the sample, measured in the calorimeter;

$Q_{эк}$ - the heat content of the electrodes, measured in the calorimeter;

$Q_{общ.к} = Q_{ок} + Q_{эк}$ - the total heat content of the sample and two electrodes, obtained from experiments;

$Q_{о} = 0{,}24\ U_{н} I_2 t_{св} cos\varphi_{н}$ - the amount of heat released in the welding section of the secondary circuit, between the electrodes, calculated from the electrical parameters of the welding process.

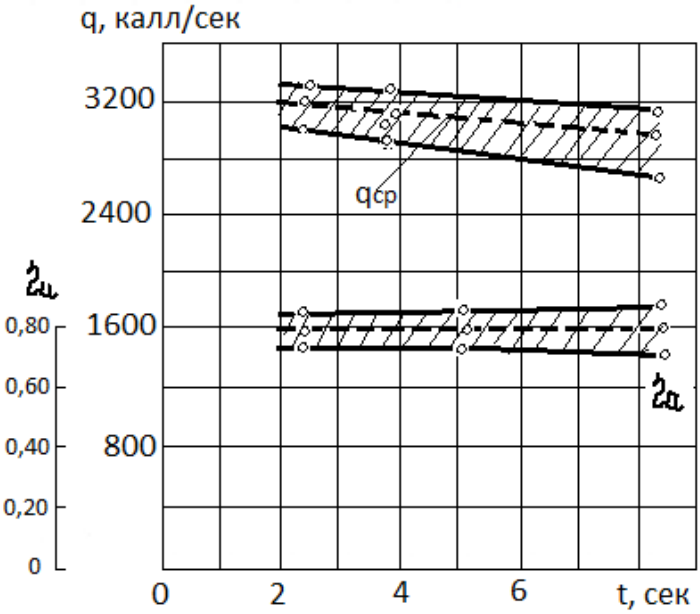

Fig. 3.13. Dependence of the average thermal power $q_{ср}$ and effective efficiency, heating process $\eta_{И}$ from the duration of the current flow I_2 = 10600 A, $U_{И}$ = 1.57 V, P = 300 dan, soft welding.

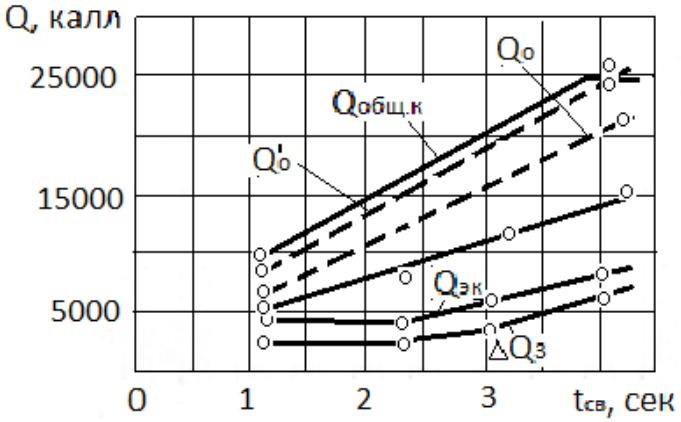

Fig. 3.14. Dependence of the heat content of samples and electrodes on the duration of heating by current at I_2 = *12900 A*, U_H = 1.788 V, P = 300 dan, hard welding mode.

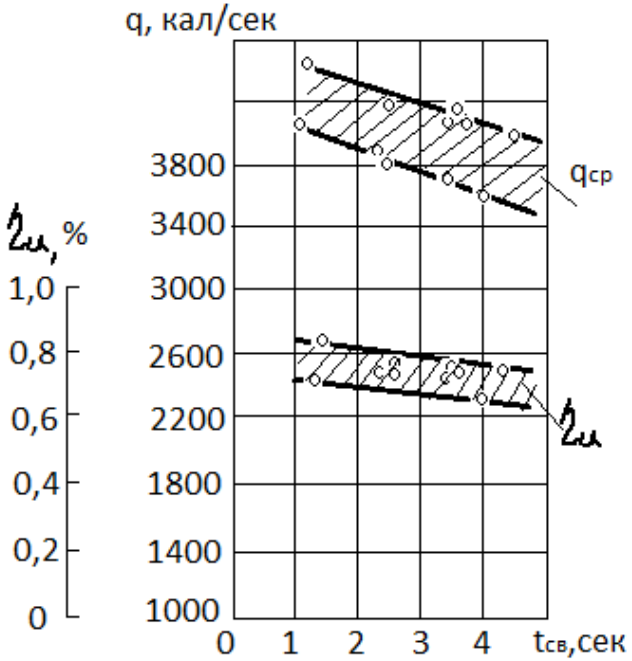

Fig. 3.15. The dependence of the average thermal power q_{cp} and effective efficiency heating process on the duration of current flow at I_2 = 12900 A, U_H = 1.788 V, P = 300 dan, hard welding mode.

$\Delta Q_э = Q_{э.к} - 0{,}24\, U_н I_2 t_{св} cos\varphi_н$- the amount of heat removed by the electrodes from the sample during welding, where $\Delta U_н = U'_н - U$ is the voltage drop across the electrodes (Fig. 3.16).

Effective efficiency heating process ηi in resistance welding of crossed rods is 0.7-0.8 with a change in current and duration of welding within the studied limits.

High value of effective efficiency can be explained by the significantly lower cooling effect of the electrodes due to their relatively large distance from the place of the greatest heating of the rods, and also due to the fact that the contact of the electrode with the rod is carried out through the surface of a relatively large area.

The longer the welding time, the lower the effective efficiency. heating process at a given current. The greater the current of a given welding duration, the lower the effective efficiency. heating process. However, at a given current, the duration of welding has a more noticeable effect on the efficiency value than the current at a given duration of welding. The average effective power of heat sources increases as the current increases, with a constant welding duration. As the duration of welding increases, the effective thermal power decreases.

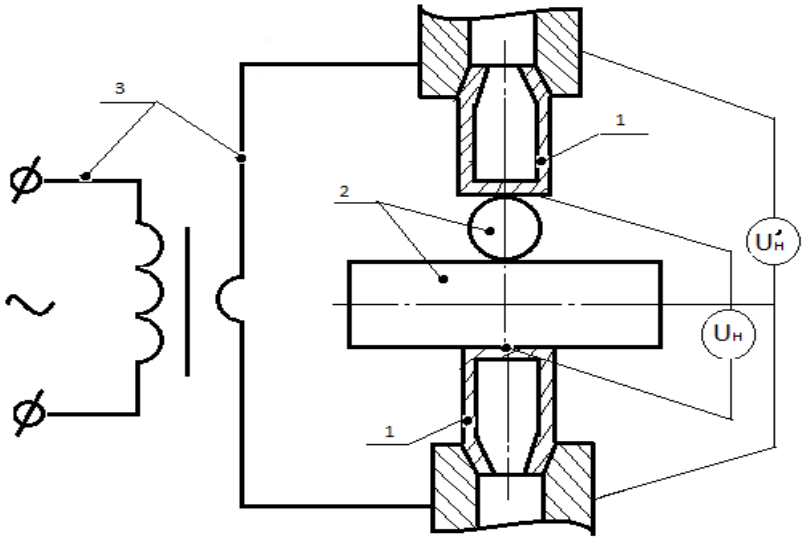

Fig. 3.16. Voltage drop measurement circuit:
1-socket electrode; 2-welded specimens; 3-welding transformer.

As a result of the analysis of the study, it was proved that the effective efficiency η and the heating process in contact welding of crossed rods is high 0.7-0.8 and the longer the duration of welding, the lower the effective efficiency. heating process.

It is also shown that the higher the current for a given welding duration, the lower the effective efficiency. welding heating process.

The ratio between the draft and the dimensions of the cold contact of the crossed rods is close to the ratio of the dimensions of the geometric elements of circular cylinders of the same diameter.

The projection area of the welding contact of the crossed rods is approximately 1.8 times larger than the projection area of the cold contact at the same upset value.

The draft is continuously calculated during the welding process, both in hard and soft welding modes, and does not stop after turning off the current.

The speed of precipitation during welding in soft mode sharply delivers at the moment the current is turned off; when welding in hard mode, the precipitation rate drops sharply even before the current is turned off.

CHAPTER 4. DETERMINATION OF PARAMETERS OF THE MODE OF ELECTROMETIC WELDING OF CROSSING ROUND RODS

As a result of the analysis of properties, alloys are divided into eight groups according to weldability [79-84]. Of these, reinforcing steels belong to the first group, the so-called low-carbon steels. Low-carbon steels with a carbon content of up to 2.5% have an average value of electrical resistivity ρ_0=13МкОм·см, low resistance to deformation, $\sigma_g = 200$ Мпа and are characterized by low sensitivity to thermal cycling and splashes.

Therefore, these steels can be welded in both hard and soft modes. Usually, one current pulse with a constant force and a simple cyclogram are used (Fig. 4.1., a, b). Based on this, when welding crossed round rods made of mild steel, the main parameters of the welding mode are:

- welding current $I_{CB;}$ *кА*;
- compression force between electrodes F_{CB}, dan;
- welding time t_{CB}, sek;
- forging force, F_K, dan;
- forging time, t_K, sek.

Since we are considering electric resistance welding of crossed round rods with a diameter of 5-10 mm, in order to obtain high-quality welding, there is no need to apply a forging force to the electrodes, therefore, the main parameters of the welding mode in our conditions are: welding current I_{CB}, compression force between the electrodes F_{CB} and welding time t_{CB}.

The welding current pulse in Fig. 4.1. is conditionally shown as a rectangle, in fact, the welding current is a sinusoid (Fig.4.2.). In calculations, we consider *I*св.д instead of Ist indicated in the figure.

For welding, electrodes with a flat working surface, electrical conductivity of at least 80% of the electrical conductivity of copper and hardness HB 120-140 are used. Usually, electrodes made of БрХ alloy are used. This alloy is copper alloyed with chromium [68, 69].

An important condition for increasing the resistance of electrodes is to reduce the temperature in the electrode-part contact.

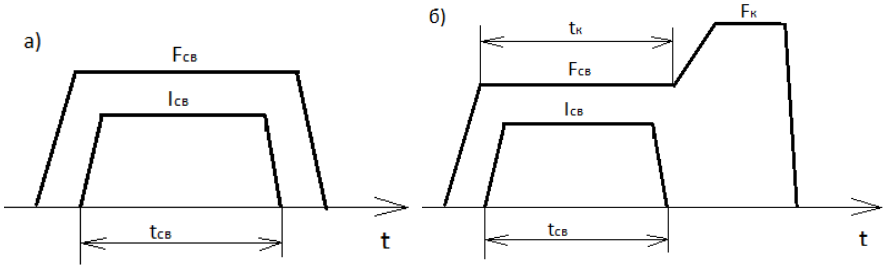

Fig. 4.1. The most common cyclograms of force and current in resistance welding of crossed round rods: *a* - with a constant welding force F_{CB}; *b* - with constant welding force and application of forging force F_K; t_K - time of application of forging force.

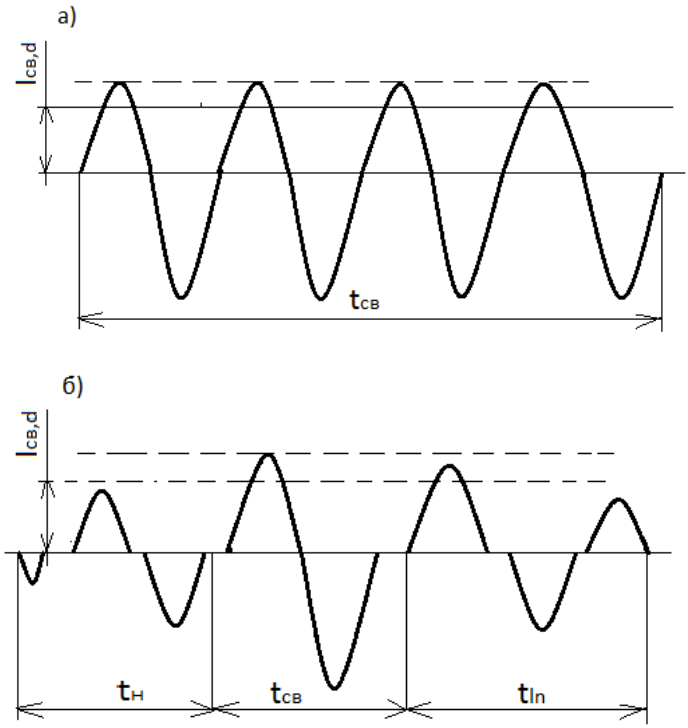

Fig. 4.2. Welding current pulse shapes:
a - alternating current; b - alternating current with modulation; tсв - instantaneous welding current; Iсв.д.- - effective welding current; tн - is the duration of the current rise; isp - the duration of the decline in the welding current.

To determine the smallest current required for welding crossed round rods, it is necessary to determine the nature of the distribution of the welding current [85-87] during welding both in the rod and in the contact being welded.

The calculation of the distribution of the transverse current in a round rod (in an armature) is reduced to solving the problem of the potential distribution in a homogeneous conducting cylinder.

With an increase in the lengths $Z_2 = Z_1$ of the source and drain contact pads with constant current densities set on them, the streamlines in the middle region adjacent to the transverse XOУ plane of source and drain symmetry deviate less and less from the transverse planes Z$= const,$, and the potential distribution in this region tends Za to a flat, not depending on the Z coordinate (Fig. 4.2).

With an unlimited increase in the lengths of the contact areas of the source and drain $2Z_2 = 2Z_1 \rightarrow \infty$ (Fig. 4.4.) And maintaining the given current planes ($j_1 = const,\ j_2 = const$) on them, the distribution of the potential and the transverse current becomes flat. The concept of total current loses its meaning in this case; it is advisable to replace it with the concept of linear current I_1 (A/cm), coming per unit length of the rod and related to the current density on the contact area by the relation

$$I_1 = 2j_1 \cdot \varphi_1 \cdot r_0 = 2j_2 \cdot \varphi_2 \cdot r_0.$$

The flat potential in a round rod, limited in length $2l$ or unlimited along its entire length, with contact pads of the source and drain, with angles of coverage φ_1 and φ_2 , is determined by the magnitude of the linear current and does not depend on the length of the rod.

To determine the nature of the distribution of the flat potential and transverse current in a round rod, we use the theory of heating rods in butt welding, proposed by Academician N.N. Rykalin. According to this theory, the heating process equation is used:

$$C\gamma(T)\frac{\partial T}{\partial t} = \frac{\partial}{\partial X}\left[\lambda(T)\frac{\partial T}{\partial X}\right] - \alpha(T)\frac{P}{F}(T - T_0) + 0{,}24\rho(T)j^2(t)[1 + \omega_k(x,t)]. \quad (4.1)$$

Using the dimensionless criteria for the heating process (4.1), the equation takes the form:

$$\frac{\partial\theta}{\partial\tau'} = \frac{\partial^2\theta}{\partial\xi^{12}} - \nu'\theta + \mu^2\vartheta^2(\theta + 1) + \omega_m\ ; \quad (4.2)$$

$$\theta(\xi', 0) = 0;$$

$$\theta(\xi^1, \tau');\ -1 \leq \xi' \leq 1;\ \ 0 \leq \tau' \leq \alpha.$$

The distribution of the flat potential U(r,φ) in a round rod loaded with a transverse linear current I1 is obtained from the expression (4.2) of the spatial potential, flattening

$$\xi_1 = \xi_2 \to \infty \qquad \text{at} \qquad \frac{I}{2\xi_1 \Gamma_0} = I_1.$$

Equation (4.2) can be easily calculated by passing to the limit under the integral sign

$$\lim_{l\to\infty} \int_0^{\infty} \frac{I_n(\omega\rho)}{\omega I_n'(\omega)} sin\omega\, \xi_{1,2} cos\omega\xi \frac{d\omega}{\omega} = \lim_{\omega\to 0} \left[\frac{I_n(\omega\rho)}{\omega I_n'(\omega)} cos\omega\xi\right] \int_0^{\infty} \frac{sinU}{U} dU =$$

$$= \frac{\omega^n \rho^n Z^n (n-1)!}{2^n n! \cdot \omega \cdot \omega^{n-1}} \cdot \frac{\pi}{2} = \frac{\pi}{2} \cdot \frac{\rho^n}{n};$$

$$U(r,\varphi) = \frac{I_1}{\pi\sigma} \sum_1^{\infty} \left\{\frac{1}{\varphi_1} cosn\left(\frac{\pi}{2} - \varphi\right) sinn\varphi_1 - \frac{1}{\varphi_2} cosn\left(\frac{\pi}{2} + \varphi_1\right) \cdot sinn\varphi_2\right\} \frac{\rho^n}{n^2}. \quad (4.3)$$

The potential is expressed as a rapidly converging power series from, the zero term of which is equal to zero, because

$$\lim_{n\to 0} \frac{1}{2} \frac{1}{n} \left[cosn\left(\frac{\pi}{2} - \varphi\right) \frac{sin\varphi_1}{n\varphi_1} - cosn\left(\frac{\pi}{2} + \varphi\right) \frac{sinn\varphi_2}{n\varphi_2}\right] = \lim_{n\to 0} \frac{1}{2n} \left[cosn\left(\frac{\pi}{2} - \varphi\right) - cosn\left(\frac{\pi}{2} + \varphi\right)\right] =$$

$$= \lim_{n\to 0} \frac{1}{2n} \cdot sin\frac{n\pi}{2} sinn\varphi = 0.$$

Thus, the potential of the center of a round rod loaded with a transverse current is equal $U(0,\varphi) = 0,$ to zero at any angles of coverage and the area of the source φ_1 and φ_2 drain.

We made this conclusion when the areas on the side of the electrode φ_1 and φ_2 the contact to be welded are not the same.

When $\varphi_1 = \varphi_2$, the potential is expressed by the following equation:

$$U(r,\varphi) = \frac{2I_1}{\pi\sigma\varphi_1} \sum_{1,3,\ldots}^{\infty} sin\frac{n\pi}{2} sinn\varphi_1 sinn\varphi \frac{\rho^n}{n^2} =$$

$$= \frac{2I_1}{\pi\sigma\varphi_1} \sum_0^{\infty} \sin(2m+1)\varphi_1 \cdot \sin(2m+1)\varphi \frac{\rho^{2m+1}}{(2m+1)^2}; \quad (4.4)$$

Here we have used the ratio

$$cosn\left(\frac{\pi}{2} - \varphi\right) - cosn\left(\frac{\pi}{2} + \varphi\right) = 2sin\frac{n\pi}{2} sinn\varphi$$

$$sin\frac{n\pi}{2}\begin{cases}0 \text{ при } n=2m\\(-1)^m \text{ при } n=2m+1\end{cases}, m=1,2,3,\dots$$

Potential (4.4) is symmetrical with respect to the horizontal axis φ=0, whose potential is equal to zero.

The distribution of the potential along the circumference of the rod at the sites with the angle of coverage $2\varphi_1 = 90^0$ calculated by (4.4) is presented in radial and rectangular coordinates (Fig. 4.5). The potential $\frac{\sigma}{I_1}U(I,\varphi)$, expressed in dimensionless units, reaches its maximum value of 0.612 at the center of the source contact area and, as it moves away from the center, decreases to 0.372 at the edge of the contact area and to zero, on the horizontal axis. The potential changes most sharply at the edge of the contact area, where the tangential component of the current density is the highest.

Let us consider the change in the potential and current density at the characteristic points of the cross section of the rod depending on the angle $2\varphi_1$ of coverage of the pads.

The greatest potential U_{Max} takes place in the center of the source site:

$$U_{\text{Max}}(\varphi_1) = U\left(I,\frac{\pi}{2}\right) = \frac{2I_1}{\pi\sigma\varphi_1}\sum_{1,3,5}^{\infty}\frac{sinn\varphi}{n^2}, \qquad (4.5)$$

because $sin^2\frac{n\pi}{2} = \begin{cases}0, \text{при } n \text{ четном}\\1, \text{при } n \text{ нечетном}\end{cases}$

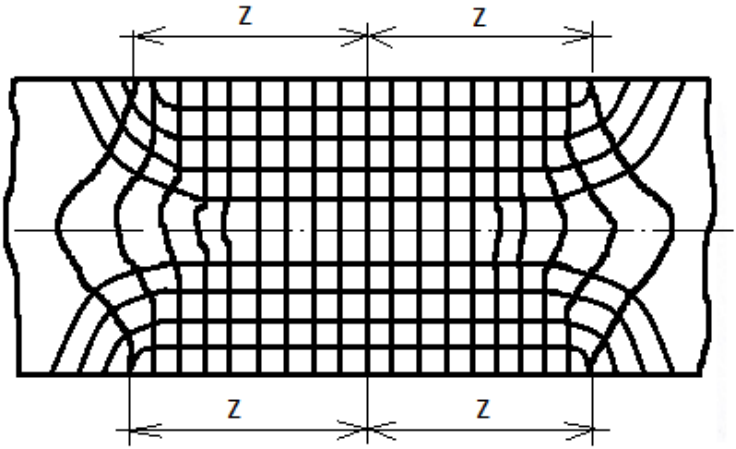

Fig. 4.3. Scheme of potential distribution in the diametrical plane of the COU with remote contact pads of the drain source

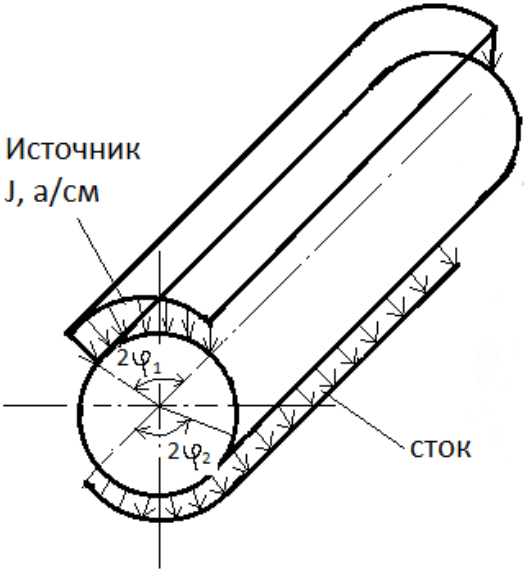

Fig. 4.4. Scheme of loading the rod with a transverse linear current

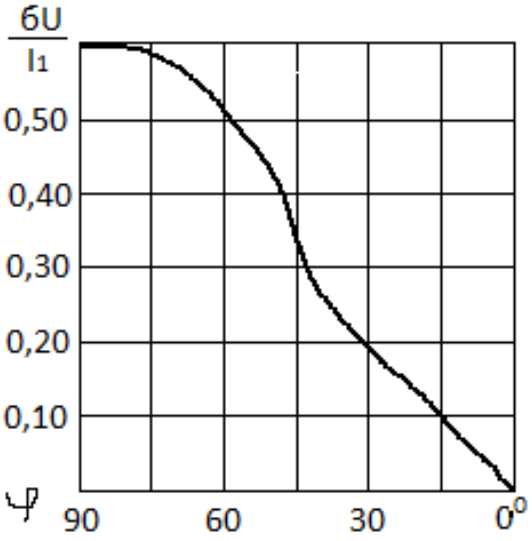

Fig. 4.5. Potential distribution around the circumference of a rod loaded with a transverse linear current I_1 with contact pads with a wrapping angle $2\varphi_1 = 90^0$

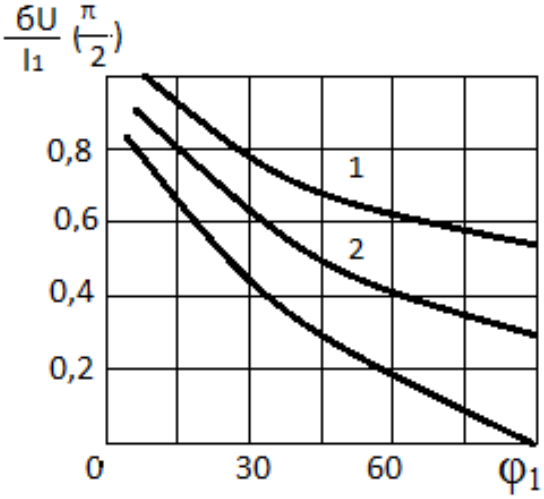

Fig. 4.6. The largest $U_{max}(1)$, smallest $U_{min}(3)$, U averaged potentials at the source site in a rod with a diameter $2r_0$ loaded with a linear transverse current, depending on the angle $2\varphi_1$ of coverage of the source or drain site.

At the edge of the source area, i.e. at $\varphi = \frac{\pi}{2} - \varphi_1$, potential

$$U\left(I, \frac{\pi}{2} - \varphi_1\right) = \frac{I_1}{\pi\sigma\varphi_1} \sum_{1,3,5}^{\infty} \frac{sin2n\varphi_1}{n^2} = U_{max}(2\varphi_1) \qquad (4.6)$$

is equal to the highest potential in the center of the site with a double angle of coverage $2\varphi_1$. Here we use the ratios

$$\sin\left(\frac{\pi}{2} - \varphi_1\right) = sin\frac{n\pi}{2} cosn\varphi_1 - cos\frac{n\pi}{2} sinn\varphi_1;$$

$$sin^2\frac{n\pi}{2} = \begin{cases} 1, \text{при } n \text{ нечетном} \\ 0, \text{при } n \text{ четном} \end{cases}$$

$$sin\frac{n\pi}{2}\ cos\frac{n\pi}{2} = 0$$

Potential averaged over the source site

$$U_{ср}(\varphi_1) = \frac{1}{\varphi_1} \int_{\frac{\pi}{2}-\varphi_1}^{\frac{\pi}{2}} U(1,\varphi)\partial\varphi = \frac{2I}{\pi\sigma\varphi_1^2} \sum_{1,3,\ldots}^{\infty} \frac{sin^2 n\varphi_1}{n^3}. \qquad (4.7)$$

Here expression (4.4) is integrated term by term under the sum sign $\frac{\pi}{2}$

$$sin\frac{n\pi}{2}\int_{\frac{\pi}{2}-\varphi_1}^{\frac{\pi}{2}} sinn\varphi\partial\varphi = \frac{1}{n}\left[cosn\left(\frac{\pi}{2}-\varphi_1\right) - cos\frac{n\pi}{2}\right]sin\frac{n\pi}{2} =$$

$$= \frac{1}{n}\ sin\frac{n\pi}{2}\left[cos\frac{n\pi}{2}\cdot cosn\varphi_1 + sin\frac{n\pi}{2}sinn\varphi_1\right] = \frac{1}{n}sinn\varphi_1$$

at n=1,3,5.

Calculated by formulas (4.5), (4.6) and (4.7) the values of the largest, smallest and average potentials at the source site, depending on the coverage angle of the site, are shown in Fig. 4.6. With a constant value of the linear current $I_1 = const$, the largest, smallest and averaged potentials decrease with an increase in the coverage angle I_1 of the source area, reaching the smallest values at the area covering the semicircle, $\varphi_1 = \frac{\pi}{2}$;

$$\frac{\sigma U_{max}(\frac{\pi}{2})}{I_1} = \frac{4}{\pi^2}\sum_{1,3,\dots}^{\infty}\frac{sin^n\frac{\pi}{2}}{n^2} = \frac{4}{\pi^2}\sum_{0}^{\infty}\frac{(-1)^m}{(2m+1)^2} = \frac{4}{\pi^2}G = 0{,}3718,$$

where $G = 0{,}916$ - constant Catalana.

$$\frac{\sigma U_{cp}(\frac{\pi}{2})}{I_1} = \frac{8}{\pi^3}\sum_{1,3,\dots}^{\infty}\frac{sin^2\frac{\pi}{2}}{n^3} = \frac{8}{\pi^3}\sum_{0}^{\infty}\frac{1}{(2m+1)^3} = 0{,}2516$$

With an unlimited decrease in the coverage angle of the site ($\varphi \to 0$), the potentials increase indefinitely.

The current density along the vertical radius of the OY is equal to the vertical component, since the horizontal component of the current density is zero$j_\rho\left(\rho,\frac{\pi}{2}\right)$,, due to the symmetry of the distribution relative to the vertical radius of the OY:

$$j_\rho\left(\rho,\frac{\pi}{2}\right) = -\frac{\sigma}{r_0}\frac{\partial}{\partial\rho}U(\rho,0) = -\frac{2I_1}{\pi\varphi_1 r_0}\sum_{1,3,\dots}^{\infty}sinn\varphi_1\frac{\rho^{n-1}}{n}. \quad (4.8)$$

Current density in the center of the rod O (Fig. 4.7, a)

$$j_\rho\left(0,\frac{\pi}{2}\right) = -\frac{2I_1}{\pi r_0}\cdot\frac{sin\varphi_1}{\varphi_1}. \quad (4.9)$$

Current density in the center of the pad

$$j_\rho\left(1,\frac{\pi}{2}\right)=-\frac{2I_1}{\pi\varphi_1\Gamma_0}\sum_{1,3,\ldots}^{\infty}\frac{sinn\varphi_1}{n}=\frac{2I_1}{\pi\varphi_1 r_0}\frac{\pi}{4}=-\frac{I_1}{2\varphi_1 r_{01}}.$$

The current density at the point (1.0) at the end of the horizontal radius OX is equal to the tangential component of the current j_φ density along the circumference of the rod $\rho = 1$ (Fig. 4.7, b)

$$j_\varphi(1,0)=-\frac{\sigma}{r_0\partial\varphi}U(1,0)=-\frac{2I_1}{\pi\varphi_1 r_0}\sum_{1,3,\ldots}^{\infty}\sin\frac{n\pi}{2}\sin\frac{n\varphi_1}{n}=-\frac{I_1}{\pi\varphi_1 r_0}\ln\frac{1+sin\varphi_1}{1-sin\varphi_1} \quad (4.10)$$

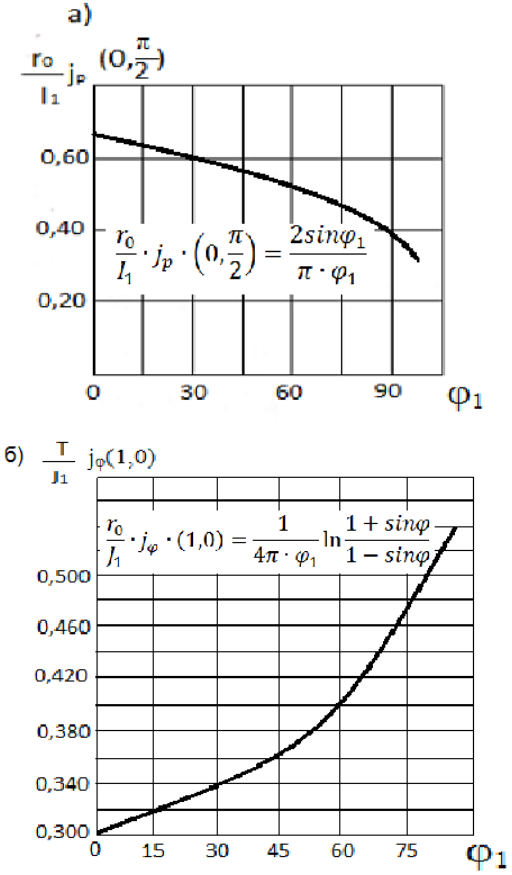

Fig.4.7. Current density in a rod with a diameter $2r_0$ loaded with linear current $I1$, depending on the angle $2\varphi_1$ of coverage of the source and drain areas:
a) in the center b) at the edge of the horizontal radius.

The minus sign in expressions (4.9) and (4.10) means that the current density vector is directed towards negative coordinates. Current density in the center (4.9) expressed in dimensionless units

$$\frac{r_0}{I_1} j_\rho(0,\frac{\pi}{2}).$$

For a given value of the linear current, I1 slightly decreases with an increase in the coverage angle $2\varphi_1$ from $\frac{2}{\pi} = 0{,}636$ at $\varphi_1=0$ to at $\frac{4}{\pi^2} = 0{,}404$, that is $\varphi_1=90°$, by only 36%. The current density (4.10) at the end of the horizontal radius, which is equal to at $\frac{1}{\pi} = 0{,}318$, increases with the angle of coverage, tending to infinity at $\varphi_1=90°$.

When the source and sink are linear, the following options are possible.

Let, at a constant value of the linear current I1, the identical contact pads decrease indefinitely ($\varphi_1 \to 0$), contracting to the generatrix of the cylinder (I, $\pm\frac{\pi}{2}$). In the limit, we obtain a cylinder loaded with a transverse current caused by a linear source along the generatrix (I, $\frac{\pi}{2}$) and a linear drain along the generatrix (I, $-\frac{\pi}{2}$).

We obtain the potential distribution by setting in expression (4.4) $\varphi_1 \to 0$ and summing the series according to the well-known relation

$$U(\rho,\varphi) = \frac{2I_1}{\pi\sigma}\sum_{1,3,\dots}^{\infty} \sin n\varphi \frac{\rho^{''}}{n} = \frac{I_1}{2\pi\sigma} \ln\frac{1+2\rho sin\varphi+\rho^2}{1-2\rho sin\varphi+\rho^2}. \quad (4.11)$$

Potential by vertical radius

$$U\left(\rho,\frac{\pi}{2}\right) = \frac{I_1}{\pi\sigma}\ln\frac{1+\rho}{1-\rho}, \quad (4.12)$$

around the circumference of the rod($\rho = 1$)

$$U(1,\varphi) = \frac{I_1}{2\pi\sigma}\ln\frac{1+sin\varphi}{1-sin\varphi} \quad (4.13)$$

increases from zero on the horizontal diameter and tends to infinity as it approaches the linear source, as where $\ln\varepsilon$, is the distance to the source $\varepsilon \to 0$.

Current density along the vertical radius

$$j_\rho\left(\rho,\frac{\pi}{2}\right) = -\frac{2I_1}{\sigma r_0}\cdot\frac{1}{1-\rho^2}. \quad (4.14)$$

And along the circumference of the rod (the tangent component, since the normal component is zero everywhere on the circle)

$$j_\rho(1,\varphi) = -\frac{1}{\pi r_0}\cdot\frac{1}{\cos\varphi}. \qquad (4.15)$$

The expression, in dimensionless units $\frac{i\mu_0}{I_1}$, increases from the values $\frac{2}{\pi}$ and $\frac{1}{\pi}$ on the horizontal diameter and, as it approaches the source, tends to infinity as ε^{-1} (Fig. 4.8).

Current density over the horizontal diameter (tangential component)

$$j_\varphi(\rho,0) = -\frac{\sigma}{r_0}\cdot\frac{\partial}{\rho\partial\rho}U(\rho,0) = -\frac{2I}{\pi r_0}\cdot\frac{1}{1+\rho^2}, \qquad (4.16)$$

expressed in dimensionless units, decreases monotonically $\frac{1}{\pi} = 0{,}636$ from the center of the rod $\frac{1}{\pi} = 0{,}318$to its circumference (Fig. 4.9).

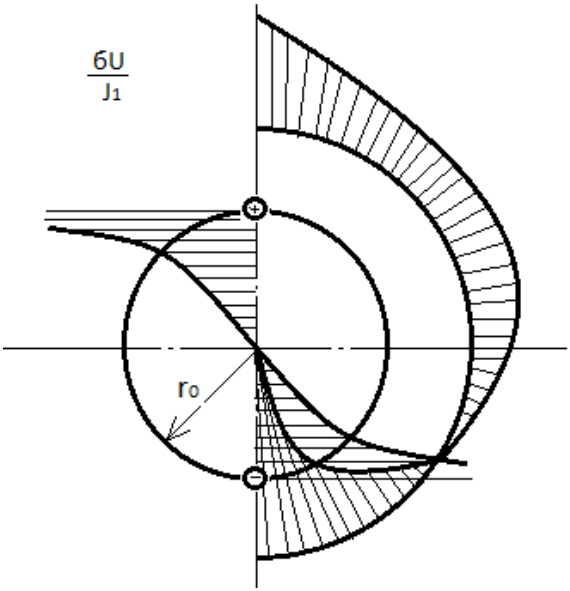

Fig. 4.8. Potential distribution along the circumference and along the vertical radius r_0 of the rod loaded with transverse current.

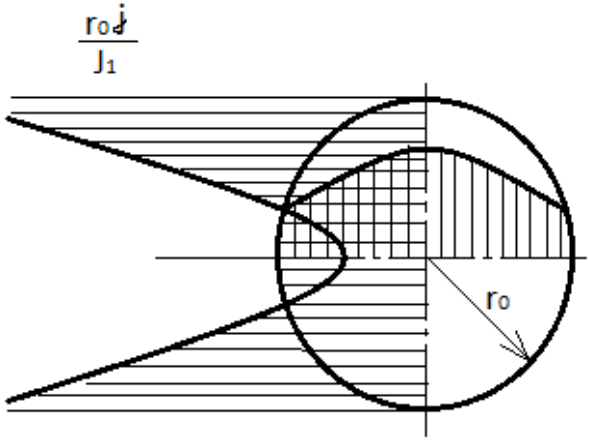

Fig. 4.9. Current density distribution around the circumference, loaded with transverse current I1.

In the previous sections, a number of issues have been considered:

- distribution of transverse current in a homogeneous round rod;
- distribution of potential and transverse current in a round rod;
- heating during contact welding of crossed rods during contact electric welding;
- experimental study of the heating process during contact electric welding of crossed round rods;
- theoretical studies of the process of heating rods;
- analysis of the heating process of the rods.

The solution of these problems made it possible to develop a method for determining the lowest current required for electric contact welding of crossed round rods.

To determine this current, we set the required maximum temperature in the contact

$$T_{max} = \frac{1}{\beta}\theta_{max}, \quad (4.17)$$

Where θ_{max} - is the maximum dimensionless temperature; β - temperature coefficient, $\frac{1}{0_C}$.

Let us assume that the required maximum temperature in the contact $\vartheta_{Nt} = 1$ is equal to the limit state temperature $\theta_{max} = \theta_{пр}$.

Then based on (2.8)

$$\theta_{max} = \frac{1 - cos\mu}{cos\mu};$$

$$T_{max} = \frac{1}{\beta} \cdot \frac{1 - cos\mu}{cos\mu};$$

where

$$\mu = arccos \frac{1}{1+\beta T_{max}} . \quad (4.18)$$

Having thus determined the value at which the specified temperature in the contact is reached, and knowing the thermophysical coefficients for a given steel grade, from expression (4.18) we find the ratio

$$\frac{I_{св}^2}{F_{пр}},$$

where I_{CE}^2 - is the smallest current required to heat the contact to a given temperature;

$F_{пр}$ - the area of the weld point (the area of the horizontal projection at the moment when the temperature in the contact reaches the limit state).

Substituting into expression (4.18) instead of its value μ

$$\mu = \frac{I_{св}}{2\pi(r_{от})_{пр}} \sqrt{\frac{0{,}24\mu\rho_0}{\lambda}};$$

we get

$$\frac{I_{св}}{2\pi(r_{от})_{пр}} \sqrt{\frac{0{,}24\mu\rho_0}{\lambda}} = arccos \frac{1}{1+\beta T_{max}};$$

where

$$\frac{I_{св}^2}{F_{пр}} = \frac{2\pi\lambda\,(arccos\frac{1}{1+\beta T_{max}})}{0{,}24\beta\rho_0},$$

where $F_{пр} = 2\pi(r_{от})^2{}_{пр}$.

Expressing $F_{пр}$ in terms of the diameter d_1 of the smaller rod, we obtain

$$\frac{I_{св}^2}{m\frac{\pi d_1^2}{4}} = (arccos\frac{1}{1+\beta T_{max}})^2 \frac{2\pi\lambda}{0{,}24\beta\rho_0}, \quad (4.20)$$

where m - ratio of area $F_{пр}$ to bar cross-sectional area $\frac{\pi d_1^2}{4}$

From expression (4.20) we have:

$$I_{св} = \pi d_1 \sqrt{\frac{m}{2} \cdot \frac{\lambda}{0{,}24 \beta \rho_0}} \cdot arccos \frac{1}{1+\beta T_{max}} . \qquad (4.21)$$

The coefficient m for a given steel grade is determined from experience $m_{min} = 0{,}6$. For mild steel m, according to our experience. The more relatively later the limit state occurs in the contact, the higher the current required for welding.

Below is an example of determining the minimum current required to weld rods with a diameter of 5 + 10 mm from mild steel:

$$d_1 = 0{,}5 \text{ см},$$
$$\rho_0 = 13 \cdot 10^{-6} \text{Ом} \cdot \text{см},$$
$$\beta = 5 \cdot 10^{-3} \, {}^1/_{{}^0\text{C}},$$
$$T_{\text{мах}} = 1500^0\text{C},$$
$$\lambda = 0{,}1 \text{ калл/см} \cdot \text{сек} \cdot {}^0\text{C},$$
$$m_{min} = 0{,}6.$$

Given these data

$$I_{min} = \sqrt{\frac{0{,}6}{2} \cdot \frac{0{,}1 \cdot 10^9}{0{,}24 \cdot 5 \cdot 13}} \cdot \pi \cdot 0{,}5 \cdot arccos \frac{1}{1+5 \cdot 10^{-3} \cdot 1500} = 2050 \text{ А}.$$

The minimum value of the current required for welding rods with a diameter of 5 + 10 mm from low-carbon steel, obtained by calculation, is close to the experimental values shown in Fig. 4.9 by linear sections.

The current density vector $j_0 = j(0,0,0)$ at the center of the rod, i.e. in the middle of the vertical diameter connecting the centers of the contact pads of the source and drain, coincides with its vertical component $j(0,0,0)$,, since the horizontal components of the current density vector are equal to zero according to the symmetry conditions. The current density in the center j_0 of the rod characterizes the degree of spreading of the transverse current along the rod. Along the horizontal diametral plane XOУ, the vertical component of the current $j_\rho(\rho, O, \xi)$ density reaches a maximum equal j_0 to O at the center.

According to the vertical diameter AB, the vertical component $j_\rho(\rho,\frac{\pi}{2},0)$ of the current density, with equal contact pads, reaches a minimum j_0 equal to O in the center; with unequal pads, the minimum current density is slightly shifted along the vertical diameter towards a larger pad.

The current density in the center $j_0(\varphi,\xi,\varphi_2,\xi_2)$ with unequal contacts of the pads is calculated by assuming the distribution of the vertical component $j_\rho(0,\frac{\pi}{2},\xi)$ of the current density along the longitudinal axis of the rod OZ:

Along the vertical diameter AB, the vertical component of the current density, with equal contact pads, reaches a minimum equal to O in the center; for unequal areas, the current density minimum shifts slightly along the vertical diameter towards the larger area.

We calculate the current density in the center with unequal contacts of the pads, assuming the distribution of the vertical component of the current density along the longitudinal axis of the rod OZ:

$$j_0(\varphi,\xi,\varphi_2,\xi_2)=j_\rho\left(0,\frac{\pi}{2},0\right)=\frac{2}{\pi^2}j_1 sin\varphi_1\int_0^\infty\frac{sin\omega\xi_1 d\omega}{\omega I_1'(\omega)}+ \tag{4.22}$$

$$+\frac{2}{\pi^2}j_2 sin\varphi_2\int_0^\infty\frac{sin\omega\xi_1 d\omega}{\omega I_1'(\omega)}.$$

With equal contact pads, the current density in the center $j_0(\varphi,\xi)$ will be obtained, flat in the expression (4.22): $j_2=j;\varphi_2=\varphi_1;\xi_1=\xi_2$.

Then both terms become equal:

$$j_0(\varphi_1,\xi_1)=\frac{4}{\pi^2}j_1 sin\varphi_1\int_0^\infty\frac{sin\varphi\xi_1 d\omega}{\omega I_1'(\omega)}\ . \tag{4.23}$$

With a point source and drain, the current density at the center $j(0,0)$ will be obtained by flattening in expression (4.23): φ_1=0 and ξ_1=0 and introducing instead of the current density in the contact area, which increases without bound, the current j_1 value I according to the relation

$$j_1=\frac{I}{4z_1\varphi_1 r_0}\quad\text{and}\quad j_2=\frac{I}{4z_2\varphi_2 r_0},$$

$$j(0,0)=\frac{I}{\pi^2 r_0^2}\int_0^\infty\frac{d\omega}{I_1'(\omega)}=\frac{k}{\pi}\cdot\frac{I}{\pi r_0}. \tag{4.24}$$

Let us calculate the integral of expression (4.24). Let us replace the derivative of the Bessel function by the value of the function itself according to the well-known relation

$$2I_n'(U) = I_{n-1}(U) + I_{n+1}(U).$$

Then

$$K = \int_0^\infty \frac{d\omega}{I_1'(\omega)} = 2\int_0^\infty \frac{d\omega}{I_0(\omega)+I_2(\omega)}. \quad (4.25)$$

The integrand of the integral (4.25) is equal to one at ω=0 and decreases with the influence of the argument, tending to zero. It is convenient to calculate the integral using the mechanical squares formula ranging from ω=0 to a sufficiently large value ω=ω1, estimating the remainder term approximately:

$$K = 2\int_0^\infty \frac{d\omega}{I_0(\omega)+I_2(\omega)} + \Delta K(\omega_1). \quad (4.26)$$

To calculate the remainder term, we use the asymmetric expansion of the Besel function

$$I_n(U) \sim \frac{1}{\sqrt{2\pi U}} e^U \left[1 - \frac{4n^2-1^2}{1!\,8U} + \frac{(4n^2-1^2)(4n^2-3^2)}{2!\,(8U)^2} - \cdots\right]$$

and restrict ourselves to two expansion terms

$$\Delta K(\omega_1) = 2\int_{\omega_1}^\infty \frac{d\omega}{I_0(\omega)+I_2(\omega)} \approx 2\sqrt{2\pi}\int_{\omega_1}^\infty \frac{e^{-\omega}\sqrt{\omega}d\omega}{\left(1+\frac{1}{8\omega}\right)+\left(1-\frac{15}{8\omega}\right)}.$$

By changing the variable $\omega = U^2$, we have

$$\Delta K(\omega_1) = 2\sqrt{\pi}\int_{\sqrt{\varphi_1}}^\infty \frac{e^{-U^2}U^2 dU}{7} \approx 2\sqrt{2\pi}\int_{\sqrt{\varphi_1}}^\infty \left(U^2+\frac{7}{8}\right)e^{-U^2}dU =$$
$$= \sqrt{2\pi\varphi_1 e^{-U_1}} + \frac{11\pi}{4\sqrt{2}}(1 - erf\sqrt{\omega_1}).$$

Expanding erf(u) into an asymptotic series and restricting ourselves to the zero and first terms, we obtain

$$\Delta K(\omega_1) \approx \sqrt{2\pi\omega_1} + \frac{11\sqrt{\pi}}{4\sqrt{2\omega_1}} e^{-\omega_1}.$$

The approximate value of K according to the Simpson formula is K = 3.55, therefore:

$$j_0(0,0) = 1{,}13\frac{I}{\pi r_0^2}.$$

The highest current density in the center $j_{0\,max}$ obviously corresponds to

$$j_{0\,max} = \frac{3{,}55}{\pi}\cdot\frac{I}{\pi r_0^2} = 1{,}33\frac{I}{\pi r_0}.$$

With unequal contact pads, the current density in the center, expressed by the relationship (4.19) and (4.20), can be represented by the half-sum current density in the center $j_0(\varphi_1, \xi_1)$ and the current density in the center $j_0(\varphi_2, \xi_2)$.

Expressing the current density $j_0(\varphi_1, \xi_1)$ and $j_0(\varphi_2, \xi_2)$, we obtain

$$j_0(\varphi_1, \xi_1, \varphi_2, \xi_2) = \frac{I}{2\pi^2 r_0^2}\left[\frac{sin\varphi_1 P(\xi_1)}{\varphi_1\ \xi_1} + \frac{sin\varphi_2 P(\xi_2)}{\varphi_2\ \xi_2}\right].$$

Thus, the calculation and analysis of the current density in the center with unequal source and sink areas is reduced to the calculation and analysis of the same value with equal areas.

Based on this, when calculating the current density in the welded rod, the conductive section is presented in the form of rectangular elements of the cylinder surface with an area

$$F_1 = 4Z_1\varphi_1 r_0,$$

F_1 - contact area between electrode and rod

$$F_2 = 4Z_2\varphi_2,$$

F_2 – area of contact between welded crossed rods.

Here, z_1 and z_2 is half the length of the contact (source and drain); φ_1 and φ_2 - half of the contact coverage angle during welding; r_0 - the radius of the cross section of the welded rod.

The current density in the center of the rod according $j_0(\varphi; \xi_1; \varphi_2; \xi_2)$, to (4.30) expressions

$$j_0(\varphi_1, \xi_1, \varphi_2, \xi_2) = \frac{I}{2\pi^2 r_0^2}\left[\frac{sin\varphi_1}{\xi_1\varphi_1}P(\xi_1) + \frac{sin\varphi_2}{\xi_2\varphi_2}P(\xi_2)\right], \quad (4.31)$$

$$\xi_1 = \frac{z_1}{r_0}; \qquad \xi_2 = \frac{z_2}{r_0};$$

$$P(\xi_1) = \int_0^{\infty} \frac{sin\omega\xi_1 d\omega}{\omega I_1'(\omega)};$$

$$P(\xi_2) = \int_0^{\infty} \frac{sin\omega\xi_2 d\omega}{\omega I_2'(\omega)};$$

$I_1'(\omega)$ - first derivative of the Bessel function of the first kind of the first order.

Consider the case of welding rods with diameters of 5+10 mm. For a rod with a diameter of 10 mm ($r_0 = 0,5$ см), the contact pads formed as a result of the crimping of the rods with a force of 300 dan before welding with a diameter of the working surface of the electrodes of 20 mm have the following dimensions (Fig. 4.10):

platform between rods:

$2Z_1$=1,0 mm; $\xi_1 = \frac{Z_1}{r_0} = \frac{0,5}{5} = 0,1;$

$2\varphi_1 r_0$=1,4 mm; $\varphi_1 = \frac{\varphi_1 r_0}{r_0} = \frac{1,4}{5} = 0,038;$

area between rods and electrode

$2Z_2$=15 mm; $\xi_2 = \frac{Z_2}{r_0} = \frac{7,5}{5} = 1,5;$ (4.32)

$2\varphi_2 r_0$=0,1 mm; $\varphi_2 = \frac{\varphi_2 r_0}{r_0} = \frac{0,05}{5} = 0,011;$

$$\frac{sin\varphi_1}{\varphi_1} \approx 1;$$

$$\frac{sin\varphi_2}{\varphi_2} \approx 1;$$

and expression (4.31) for this case will take the following form:

$$j_0(\xi_1, \xi_2) = \frac{I}{2\cdot\pi^2\cdot {r_0}^2}\left[\frac{P(\xi_1)}{\xi_1} + \frac{P(\xi_2)}{\xi_2}\right], \quad (4.33)$$

those. for given dimensions of the pads, the current density of the rod depends mainly on the longitudinal dimensions of the pads (ξ1 and ξ1), while the transverse dimensions ($\varphi_1 r_0$ и $\varphi_2 r_0$) can be neglected.

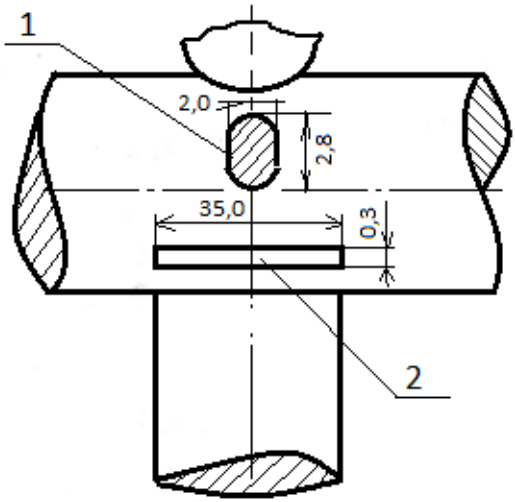

Fig. 4.10. The layout of the contact pads on the surface of the rod:
1- contact area between the rods; 2- contact pad between the rod and the electrode.

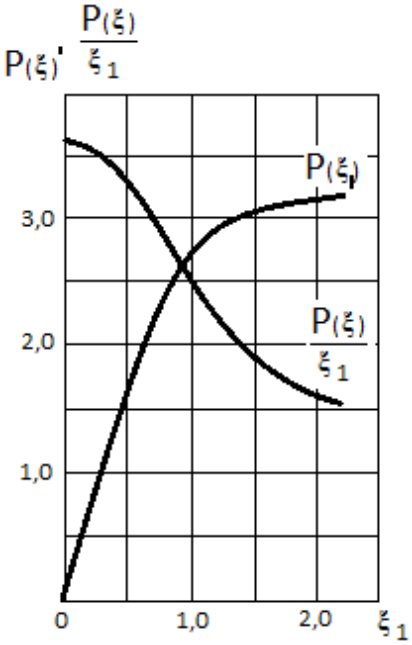

Fig.4.11. Ratio of P(ξ) from ξ1.

Thus, the pads in this case can be considered as a linear current source and a drain of finite length on the surface of a non-contact round rod.

Putting the values ξ1 and ξ2 from (4.32) into expression (4.33), and $r_0 = 0{,}5$ см, we get

$$j_0(\xi_1, \xi_2) = \frac{J_2}{2 \cdot \pi^2 \cdot 0{,}5^2}\left[\frac{P(0{,}1)}{0{,}1} + \frac{P(1{,}5)}{1{,}5}\right].$$

Values $\frac{P(0,1)}{0,1}$ and $\frac{P\,(1{,}5)}{1{,}5}$ take from Fig.4.11

$$\frac{P(0{,}1)}{0{,}1} = \frac{0{,}35}{0{,}1} = 3{,}5;$$

$$\frac{P\,(1{,}5)}{1{,}5} = \frac{3{,}0}{1{,}5} = 2{,}0;$$

$$j_0(\xi_1, \xi_2) = \frac{J_2}{2 \cdot \pi^2 \cdot 0{,}5^2}(3{,}5 + 2{,}0) = 5{,}5\,\frac{J_2}{2 \cdot \pi^2 \cdot 0{,}5^2}. \qquad (4.34)$$

Let us calculate the current density in the center of a large rod according to this scheme, applying the conditions that the rods are made of St3

$$\rho_0 = 13 \cdot 10^{-6}\ \text{Ом} \cdot \text{см};$$

$$C\gamma = 0{,}79\ \text{кал/см}^3{}^0\text{C};$$

current at the beginning of the process

$$J_2 = 2100\ \text{А}.$$

Line sources and sink

$$j_0(\xi_1, \xi_2) = 5{,}5 \cdot \frac{2100}{2 \cdot \pi^2 \cdot 25} = 5{,}5 \cdot \frac{2100}{2 \cdot 3{,}14^2 \cdot 25} = \frac{11550}{560} = 23{,}1\,\frac{\text{А}}{\text{мм}^2}.$$

Pressure in the contact zone during welding

$$\text{К} = \frac{\text{Р}}{F}\ \frac{\text{дан}}{\text{мм}^2} = 5{,}5\ \frac{\text{дан}}{\text{мм}^2}.$$

Estimated value of the site in the contact zone

$$F = \frac{2100\ a}{231{,}0\ a/\text{см}^2} = 90{,}9\ \text{мм}^2.$$

Compression force between electrodes

$$P_{св} = K \cdot F = 5{,}5 \cdot 90{,}9 = 500\ \text{дан}.$$

CONCLUSIONS

In industrial and civil construction, in widespread structures made of unstressed reinforced concrete, class B-1, Vr-1 reinforcement is used. Often it is a so-called. a metal mesh made of smooth wire with a diameter of 3-5 mm, both of the same and different sections.

Statistical analysis of the parameters of the modes used in production conditions, as well as studies have shown: in the production of building reinforced concrete structures in the manufacture of metal meshes, there is an excessive consumption of electricity.

This can be avoided by reducing the welding current in such a way that the necessary strength of the weld point is provided, corresponding to the linear section of the change in strength from the welding current.

The highest heating rates occur in the initial stage of the process. When welding in soft and hard modes, the zone of the near-contact area is heated to the melting temperature within 1.5-2 seconds. In the subsequent stage of heating and with an increase in the contact area between the connected rods, the heating process in the near-contact region tends to the limiting state.

The temperature of the points near the contact area on the side of the rod of small radius is 100-150°C higher than on the side of the rod of large radius.

The level of the area of limiting temperatures in the zone of welding contact can be controlled by various combinations of force on the electrodes and the electrical parameter of the process, but not by the duration of welding.

The values of the maximum temperatures of points remote from the welding contact for a given combination of force on the electrodes and the electrical parameters of the welding mode are controlled by the duration of the current flow.

The higher the current during welding, the relatively later the limit state occurs, the shorter the duration of welding and the less the possibility of overheating of the near-contact area. That is, it is desirable to weld the rods in a hard mode.

As a result of the analysis of the study, it was proved that the effective efficiency η and the heating process in contact welding of crossed rods is high 0.7-0.8 and the longer the duration of welding, the lower the effective efficiency. heating process.

It is also shown that the higher the current for a given welding duration, the lower the effective efficiency. welding heating process.

The ratio between the draft and the dimensions of the cold contact of the crossed rods is close to the ratio of the dimensions of the geometric elements of circular cylinders of the same diameter.

The area of the projection of the welding contact of the crossed rods is approximately 1.8 times larger than the area of the projection of the cold contact at the same value of settlement.

The draft is continuously calculated during the welding process, both in hard and soft welding modes, and does not stop after the current is turned off.

The precipitation rate during welding in soft mode sharply delivers at the moment the current is turned off; when welding in hard mode, the precipitation rate drops sharply even before the current is turned off.

Study of the process of electric contact welding of crossed round rods, i.e. reinforced concrete reinforcement, showed:

- the dimensions and shapes of the contact depend on the dimensions and shapes of the rods and electrodes, as well as on the compression force between the electrodes;

- the area of contact between the welded rods depends on the draft during welding Fw(h) and during cold bending of the rods Fx(h)

$$Fсв(h) = 1,8\ Fx(h);$$

- when welding rods in the contact zone, the specific pressure has a constant value and depends on the hardness of the rod material

$$K \approx 0,6HB;$$

but when welding rods of small diameter (up to 5 mm)

$$K \approx 1,28HB.$$

The pattern of temperature change in the welding zone is experimentally determined. It was found that the required heating rates take place at the initial stage of the process. The point of the near-contact area is heated to the melting temperature of the base metal within 1.5-2 sec.

The limiting temperature of the points of the near-contact area on the side of the small rod is 100-150º C higher than on the side of the large rod.

It has been established that the longer the duration of welding, the lower the effect of the heating process. At a given current value, it is proposed to carry out welding of crossed round rods in a hard mode (tw<4sec).

It has been established that the current density in the central part of the contact depends only on the length of the contact between the welded rods, as well as on the length of the contact between the electrodes of the rod.

On the basis of the experiments carried out and comparison of the experimental data with the results of calculating the temperature of the near-contact region in the limiting state, a method is proposed for determining the lowest current required for welding rods.

A technique has been developed for determining the compression force between the electrodes in the center of the welding contact, taking into account the required minimum welding current of crossed round rods.

LITERATURE

1. Technology of concrete of building products and structures: methodological guidelines for the implementation of course work for full-time and part-time students of specialty 290600 /Comp. D.I. Gladkov. – Belgorod: Publishing House of V.G. Shukhov BSTU, 2005. – 24 p.
2. Prykin B.V. Design and optimization of technological processes of precast concrete plants. – Kiev: Vishcha shkola, 1976. - 302 p.
3. Prykin B.V., Boyko V.E., Drobot V.V. Technological design of reinforcement production. – Kiev: Budivelnik, 1977. – 196 p.
4. Bazhenov Yu.M., Komar A.G. Technology of concrete and reinforced concrete products. – M.: Stroyizdat, 1984. – 671 p.
5. Gershberg O.A. Technology of concrete and reinforced concrete products. – M.: Stroyizdat, 1971. – 359 p.
6. ONTP-07-85. All-Union norms of technological design of precast concrete enterprises. – M.: Higher School, 1986. – 51 p.
7. Handbook on the production of precast concrete products. /Edited by K.V. Mikhailov et al. – M.: Stroyizdat, 1982. – 440 p.
8. Baykov V.N., Sigalov E.E. Reinforced concrete structures. General course. Ed. 4-E. – M.: Stroyizdat, 1991. – 767 p.
9. Baykov V.N., Drozdov P.F., Trofimov I.A., etc. Reinforced concrete structures. Special course. – M.: Stroyizdat, 1981. - 768 p.
10. Murashev V.I., Sigalov E.E., Baykov V.N. Reinforced concrete structures. General course. – M.: Gosstroizdat, 1962. – 660 p.
11. Rivkin S.A., etc. Reinforced concrete structures (calculation and construction). /Edited by S.A. Rivkin. 3rd Ed., reprint. and additional – Kiev: Budivelnik, 1973. – 875 p.
12. Gvozdev A.A., Dmitriev S.A., Gushcha Yu.P., etc. New in the design of concrete and reinforced concrete structures. /Edited by A.A. Gvozdev. – M.: Stroyizdat, 1978. – 208 p.
13. Tsai T.N. Building structures. In 2 volumes. – M.: Stroyizdat, 1985. – 462 p.
14. Guide to the construction of concrete and reinforced concrete structures made of heavy concrete (without prestressing). Leningrad: Promstroyproekt TsNII promzdanii, NIIZhB. – M.: Stroyizdat, 1978. – 129 p.
15. Vakhnenko N.F., Mogilat A.N. et al. Building structures of buildings and structures. Stroyizdat, M., 1980. – 423s.
16. Sekhniashvili E.A. Engineering method for calculating elastic systems for free vibrations. – Tbilisi: Tsodna, 1960. - 345 p.
17. Kalnitsky A.A., Peshkovsky L.M. Calculation and construction of reinforced concrete foundations of civil and industrial buildings and structures. – M.: Higher School, 1974. – 264 p.

18. Typical reinforced concrete structures of buildings and structures for industrial construction. /Edited by G.I. Berdichevsky. – M.: Stroyizdat, 1981. – 489 p.
19. Axelrod F.A., Mirkin A.M. Equipment for contact welding: Handbook. – M.: Mechanical Engineering, 1979. – 70 p.
20. Moravsky V.E., Vorona D.S. Technology and equipment for point and relief condenser welding. – Kiev: Naukova dumka, 1985. – 272 p
21. Chuloshnikov P.L. Spot and roller electric welding of alloy steels and alloys. – M.: Mechanical Engineering, 1974. – 232 p.
22. Paton B.E., Lebedev V.K. Electrical equipment for contact welding. – M.: Mechanical engineering, 1969. – 440 p.
23. Nikolaev G.A., Kurkin S.A., Vinokurov V.A. Calculation, design and manufacture of welded structures. – M.: Higher School, 1971. – 760 p.
24. Lviv N.S., Gladkov E.A. Automation and automation of welding processes. – M.: Mechanical Engineering, 1982. – 301 p.
25. Kuchuk-Yatsenko S.N., Lebedev V.K. Contact butt welding by continuous reflow. – Kiev: Naukova dumka, 1976. – 215 p.
26. Welding quality control. /Edited by V.N. Volchenko. – M.: Mashinostroenie, 1975. –328s.
27. Gulyaev A.I. Technology of spot and relief welding of steels. – M.: Mechanical Engineering, 1978. – 244 p.
28. Theoretical foundations of welding. / Edited by V.V. Frolov. – M.: Higher School, 1970. – 592s.
29. Isaev A.P., Shashin D.M., Shalamberidze M.Sh. Assessment of the strength of the welded assemblies of small-sized relays according to the parameters of the condenser welding process. /Proceedings of the Moscow State Technical University, No. 363, Moscow, 1981, pp.66-72.
30. Isaev A.P., Shashin D.M., Shalamberidze M.Sh. Scheme of mechanical tests for assessing the quality of welded joints of small-sized parts. /Izv. Universities. Mechanical Engineering, No.3, Moscow, 1982, pp.105-109.
31. Shalamberidze M.Sh., Moiseenko D.B., Isaev A.P. Evaluation of the quality of welded joints of relay assemblies performed by capacitor welding using a generalized indicator. /Proceedings of MVTU, No. 434, Moscow, 1985, pp.60-67.
32. Shalamberidze M.Sh. Mathematical model of contact spot welding. /Proceedings of the Georgian Technical University, Tbilisi, No. 2 (418), pp.42-46.
33. Sulamanidze A.K., Shalamberidze M.Sh., Darchiashvili Ts.M., Konava Zh.Zh. Influence of the shape of the welded part on the formation of the cast core. /Georgian Engineering News, No.1 (Vol. 49), 2009, pp.80-85.
34. Shalamberidze M.S. Questions of modeling contact spot welding. /Proceedings of the Georgian Technical University, Tbilisi, No.4 (418), pp.42-46.

35. Pustilnik E.I. Statistical methods of analysis and processing of observations. - M.: Nauka, 1968. – 288 p.
36. Shalamberidze M.Sh. Prediction of outbursts in the process of capacitor welding by moving a movable electrode. /Proceedings of the Georgian Polytechnic Institute, No.13 (310), Tbilisi, 1986.- 68-73 p.
37. Shalamberidze M.S. Algorithm for quality control of magnetic relay system type RES./Proceedings of the Georgian Polytechnic Institute, №13 (310), Tbilisi, 1986.- 64-68 p.
38. Akimenko A.D. Heat exchange processes in the production of a continuous steel ingot. /Proceedings on Mechanical Engineering and Metallurgy, 1960, 20, Issue 1, 15-18 p.
39. Budak B.M., Solovieva E.V., Uspensky A.B. Difference method with smoothing coefficients for solving the problem. /Journal of Computational Mathematics and Mathematical Physics, 1965, 5 No.5, 75-78 p.
40. Gradshtei I.S., Ryzhik I.M. Tables of integrals, sums and series. – M.: Gostekhizdat fiz-mat. Lit., 1963.-1108 p.
41. Brodsky A.Ya. On the parameters of the mode of contact electric welding of intersecting rods of reinforced concrete structures. /Automatic welding, No. 1, 1954.
42. Volchenko V.N., Kosyrev V.F., Evgeniev I.E. Choice of spot welding mode of intersecting reinforcement rods. / Welding production, No. 10, 1956.
43. Rykalin N.N. Heating of rods by current when welding into a joint with resistance. /Welding production, No. 4, 1967.
44. Adasinsky S.A. Cooling of thin steel sheets during spot welding. /Welding production, No. 8, 1955.
45. Rykalin N.N., Pugin A.I. The effect of the surface effect on the heating of steel rods during contact butt welding. /Welding production, No. 4, 1954.
46. T. Okamoto. Electrical resistance welding. – M.: Orgametall, 1956.
47. Kochergin K.A. The choice of contact welding technology. – L.: Sudpromgiz, 1958.– 60 p.
48. Pugin A.I. The effect of the surface effect on the heating of steel rods during contact butt welding. /Welding production, No. 7, 1959.-65 p.
49. Shalamberidze M.Sh., Khvadagiani A.I., Tskalobadze A.P., Sakhvadze D.V. Method of manufacturing electrodes for electrocontact spot welding. Author's certificate of the USSR No. 1660902, B23KM130. Priority of the invention July 6, 1989 0707.91. Bulletin No. 25.
50. Pkhakadze T.I., Shalamberidze M.Sh., Mgaloblishvili K.D., Dadunashvili G.G. Determination of welding current in contact multipoint welding. /Measuring Equipment Magazine Vol. 53, №8, 2010.- 55-57 p.
51. Gray E., Matthews B.T. Bessel functions and their application to physics and mechanics. – M.: 1959.

52. Ospanova S., Zivzivadze L., Shalamberidze M. On the issue of developing an energy-saving technology for welding rebar from crisscrossing round rods. /III International Scientific Conference "Energy: regional problems and development prospects", Kutaisi, 2015.10.24-25. - 237-241 p.
53. Ospanova S., Zivzivadze L., Shalamberidze M. Features of the development of energy-saving technology for the manufacture of metal mesh. / “Georgian Engineering News", Tbilisi, 2014, 48-51 p.
54. Selection of criteria for assessing the quality of electrocontact welding of reinforced concrete reinforcement. / “Georgian Engineering News", Tbilisi, 2015, 48-50 p.
55. Ospanova S., Khvadigiani A., Shalamberidze M. Experimental study of the heating process during electric contact welding of intersecting round rods. / “Georgian Engineering News", Tbilisi, 2015.- 80-83p.

APPENDIX

Examples of calculating the parameters of the welding mode of crossed round rods of small diameter.

An example of determining the minimum current required for welding rods with a diameter of 3 + 5 mm from mild steel.

As a result of the analysis of calculations of thermal processes during welding of crossed round rods, as well as the studies of the temperature field during welding, the following dependence for determining the welding current was obtained:

$$I_{св} = \pi d_1 \sqrt{\frac{m}{2} \cdot \frac{\lambda}{0{,}24\beta\rho_0}} \cdot arccos \frac{1}{1+\beta T_{max}}$$

The coefficient m for mild steel is determined experimentally and according to our experiments for welding rods of small diameter m=0.6.

And the larger its value, the relatively later the temperature limit state occurs in the welding contact and the higher the current required for welding. When welding in a pair of rods of different diameters, the welding mode is determined by rods of small diameter, therefore, to calculate the welding current in this case, we take $d_1 = 0{,}3$ cm.

For mild steel

$$T_{max} = T_{пл} = 1500^0\text{C}$$

Resistivity of rods

$$\rho_0 = 13 \cdot 10^{-3}\,\text{Ом} \cdot \text{см}$$

Temperature coefficient

$$\beta = 5 \cdot 10^{-3}\ 1/0\text{C}$$

Coefficient of thermal conductivity

$$\lambda = 0{,}1\ \text{ккал/см} \cdot \text{сек}\ 0\text{C}$$

Given these data

$$I_{св} = \sqrt{\frac{0{,}6}{2} \cdot \frac{0{,}1 \cdot 10}{0{,}24 \cdot 5 \cdot 10^{-3}}} \cdot \pi \cdot arccos \frac{1}{1 + 5 \cdot 10^{-3} \cdot 1500} = 1950\ \text{А}.$$

An example of determining the compression force between the electrodes.

As a result of the calculation, analysis of the electric field and current density when welding crossed round rods, it was found that the current density

$$j_0(\xi_1, \xi_2) = \frac{I}{2\pi r_0^2}\left[\frac{P(\xi_1)}{\xi_1} + \frac{P(\xi_2)}{\xi_2}\right]$$

Those, for given dimensions of the pads, the current density of the rod depends mainly on the longitudinal dimensions of the pads ξ_1 and ξ_2.

$$\xi_1 = \frac{Z_1}{r_0}$$

$$\xi_2 = \frac{Z_2}{r_0}$$

r_0 - rod cross section radius;

Z_1 - the size of the imprint along the abscissa between the rods during cold crimping;

Z_2 - the size of the imprint crumpling between the electrodes and the rod.

With cold bending of the rods 3 + 5 mm (at a pressure of 500 dan)

$$Z_1 = 0{,}5 \text{ мм}$$

$$Z_2 = 5 \text{ мм}$$

Respectively

$$\xi_1 = \frac{0{,}5}{2{,}5} = 0{,}2$$

$$\xi_2 = \frac{5}{2{,}5} = 2{,}0$$

Values

$$\frac{P(0{,}2)}{0{,}2} = \frac{0{,}5}{0{,}2} = 2{,}52$$

$$\frac{P(2{,}0)}{2{,}0} = \frac{3{,}25}{2{,}0} = 1{,}625$$

Let's take from Fig. 4.11. current density:

$$j = \frac{1950}{2\pi r_0^2}[2{,}5 + 1{,}625] = \frac{1950}{2\pi 1{,}5^2} \cdot 4{,}125 = \frac{8043{,}75}{44{,}3682} = 569{,}3\text{Δ/мм}^2$$

because $j = \frac{I}{j} = \frac{1950}{569{,}3} = 3{,}4$

Specific pressure

$$\text{К} = 1{,}28\ \text{НВ}; \quad \text{К} = 1{,}28 \cdot 146{,}6 = 187{,}6\ \text{дан/мм}^2$$

$$\text{К} = \frac{P}{S} = 146{,}6 \cdot 1{,}28 = 187{,}6\text{дан/мм}^2$$

Force between electrodes

$$P = K \cdot S = 187{,}6 \cdot 3{,}4 = 600\ \text{дан}$$

Thus, the welding mode parameters are:

$$I_{\text{св}} = 1950\ \text{А}; \quad \text{Р} = 600\ \text{дан}; \quad t_{\text{св}} \leq 4\ \text{сек}.$$

ENERGY-SAVING TECHNOLOGIES MANUFACTURING OF METAL STRUCTURES WITH CORE ELEMENTS

MONOGRAPH

S. M. Ospanova

Passed for printing 12.05.2022. Appearance 17.05.2022.
Typeface Times New Roman. Circulation 100 copies.
RS Global Sp. z O.O., Warsaw, Poland, 2022
Numer KRS: 0000672864
REGON: 367026200
NIP: 5213776394

ENERGY-SAVING TECHNOLOGIES MANUFACTURING OF METAL STRUCTURES WITH CORE ELEMENTS

S. M. OSPANOVA

RS Global

Publisher:
RS Global
Dolna 17, Warsaw,
Poland 00-773
https://monographs.rsglobal.pl/
Tel: +48 226 0 227 03
Email: monographs@rsglobal.pl